Geological Society of America
Special Paper 410
2006

Petrology and geochemistry of the Middle Jurassic Ironside Mountain batholith: Evolution of potassic magmas in a primitive arc setting

Calvin G. Barnes*
Elizabeth V. Mars
Department of Geosciences, Texas Tech University, Lubbock, Texas 79409-1053, USA
Susan Swapp
Carol D. Frost
Department of Geology and Geophysics, Dept. 3006, 1000 E. University Avenue, University of Wyoming, Laramie, Wyoming 82071, USA

ABSTRACT

The Ironside Mountain batholith consists of the 170-Ma Ironside Mountain pluton, the quartz diorite of Happy Camp Mountain, the 167-Ma Denny intrusive complex, and the West China Peak intrusive complex. The contact aureole of the Ironside Mountain pluton is present in both the western and eastern Hayfork terranes, which indicates that emplacement followed regional thrusting along the Wilson Point thrust. The batholith marks the beginning of a 15-m.y.-long episode of arc magmatism. Al-in-hornblende barometry suggests emplacement at ~4 kb. The Denny and West China Peak complexes are predominantly gabbro to olivine pyroxenite characterized by calcic plagioclase. Along with the quartz diorite of Happy Camp Mountain, these plutons have calcic bulk compositions, abundant amphibole, and low FeO/(FeO + MgO). Their chemical and petrographic features suggest oxidized, H_2O-rich parental magmas. In contrast, the Ironside Mountain pluton has higher FeO/(FeO + MgO), shows K_2O enrichment with increasing SiO_2 to ultrahigh-K compositions, and is typified by 2- and 3-pyroxene assemblages in which hydrous mafic silicates are sparse or absent, except in the most evolved rocks. The elements Rb, Zr, and Ba all behave incompatibly. Initial Nd and Sr isotope ratios (170 Ma) are uniform at ε_{Nd} of ~5.2 and $^{87}Sr/^{86}Sr$ of ~0.7037. These data suggest that the pluton lacks significant crustal input, unlike younger Middle Jurassic plutons, and that it evolved primarily by fractional crystallization of a reduced, H_2O-poor arc tholeiite. Enrichment of K_2O is interpreted to result from differentiation at relatively high pressure (≥8 kb), under conditions in which augite fractionation predominated over olivine fractionation. High-P fractionation without appreciable crustal input is probably related to the thermal structure of the crust. Emplacement immediately after regional thrusting placed parental magmas into cool, nonreactive host rocks. Succeeding Middle Jurassic magmatism encountered progressively hotter crust, with consequent crustal melting and assimilation.

Keywords: Klamath Mountains, arc magmatism, Jurassic, potassic

*E-mail: Cal.Barnes@ttu.edu.

Barnes, C.G., Mars, E.V., Swapp, S., and Frost, C.D., 2006, Petrology and geochemistry of the Middle Jurassic Ironside Mountain batholith: Evolution of potassic magmas in a primitive arc setting, *in* Snoke, A.W., and Barnes, C.G., eds., Geological studies in the Klamath Mountains province, California and Oregon: A volume in honor of William P. Irwin: Geological Society of America Special Paper 410, p. 199–221, doi: 10.1130/2006.2410(10).

INTRODUCTION

Mesozoic volcanic and plutonic rocks in the Klamath Mountain province have long been considered to be excellent examples of primitive arc magmatism (Moore, 1959; Hotz, 1971; Irwin, 1972). Most of these rocks are calcic or calc-alkaline (Hotz, 1971; Barnes et al., 1992). However, Lanphere et al. (1968) and Hotz (1971) recognized a group of plutons with unusual K_2O-rich compositions. In modern terminology, these are plutons with evolved rock compositions in the monzonitic and quartz monzonitic range, rather than in the tonalitic and granodioritic range. The Ironside Mountain batholith and the Wildwood pluton are the largest examples of these K_2O-rich plutons (Hotz, 1971), and the Ironside Mountain batholith is the subject of this chapter. It is the largest plutonic unit in the Klamath province, with a length of 72 km and a maximum width of 12 km.

The Ironside Mountain and Wildwood plutons have radiometric ages in the 169- to 170-Ma range (Wright and Fahan, 1988) and on the basis of these ages and earlier K-Ar and Rb-Sr geochronology (Lanphere et al., 1968), Irwin and Wooden (1999) defined a "Western Hayfork" magmatic episode that encompassed the previously mentioned plutons, the western Hayfork terrane, and a number of small plutons with similar ages throughout the province. One of the principal assumptions of this grouping is that Ironside Mountain–type plutons are the intrusive equivalents of the western Hayfork terrane volcanic and volcaniclastic strata. Geologic data presented here show that this interpretation must be reconsidered. Furthermore, we show that Ironside Mountain–type magmatism is unusual relative to other Klamath plutonism and that it occurred in a specific, postcontractional tectonic setting. In this chapter, we describe the Ironside Mountain batholith, its contact relations, mineral assemblages, and geochemical composition. We then propose a petrogenetic model for its origin.

METHODS

The first detailed field study of the Ironside Mountain batholith was part of the Ph.D. dissertation of D. Charlton (1979). He mapped the rugged central part of the batholith and its host rocks. He interpreted the main plutonic unit to be crudely zoned, and he also mapped several small, compositionally distinct intrusive bodies within or adjacent to the main unit. Our work extended Charlton's mapping to the north and south. Particularly in the south, much of the pluton is poorly exposed, such that exposures were limited to road cuts. However, glaciated exposures in the northeastern part of the pluton permitted inspection of larger, more continuous outcrops.

Bulk geochemical analysis was done at Texas Tech University by inductively coupled plasma atomic emission spectrometry for major elements, plus Sr, Zr, Y, Nb, Ba, Sc, Cu, Cr, and Zn. The element Rb was analyzed by flame emission. For samples whose sample number ends in "91," the rare-earth elements, Th, Ta, and Hf, were analyzed by instrumental neutron activation analysis at Oregon State University. Rare-earth element concentrations in samples whose numbers end in "88" were determined by inductively coupled plasma emission spectroscopy after separation by ion exchange methods (see Shannon et al., 1997). These data were supplemented by analyses from Lanphere et al. (1968) and Charlton (1979).

Mineral compositions were analyzed on an automated JEOL 8900 Superprobe at the University of Wyoming. Nominal instrument conditions were 15-kV accelerating potential and a beam current of 10–20 nA. Standards were natural and synthetic silicates and oxides; data were reduced using ZAF corrections.

The original Sr isotopic data were produced by R.W. Kistler at the U.S. Geological Survey. More recent data were collected at the University of Wyoming, where bulk rock Nd and Sr isotopic compositions were determined by thermal ionization mass spectrometry. The Sm, Nd, Rb, and Sr concentrations were determined by isotope dilution on aliquots of the same sample dissolved for isotope ratio measurements. See Table 7 for analytical details.

GEOLOGIC SETTING

Regional Geology

The Ironside Mountain batholith intruded a stack of imbricate tectonostratigraphic terranes separated by east-dipping thrust faults (e.g., Irwin, 1972; Charlton, 1979; Wright, 1982). From structurally lowest, these are the Rattlesnake Creek terrane, the western Hayfork terrane, and the eastern Hayfork terrane (terminology of Wright, 1982; Fig. 1). All of these units and the batholith were thrust over the Galice Formation during the Nevadan orogeny (e.g., Harper and Wright, 1984).

West of the Ironside Mountain batholith, the Galice Formation consists primarily of semipelitic slate and phyllite, with lesser amounts of chlorite-rich phyllite, greenschist, and minor greenstone (Young, 1978). To the north, the Galice Formation contains ca. 153-Ma detrital zircons (Miller et al., 2003) and is cut by dikes and plutons as old as 151 ± 2 Ma (Saleeby et al., 1982; Harper et al., 1994).

The Rattlesnake Creek terrane consists of a lower ophiolitic mélange that is locally unconformably overlain by coherent metasedimentary and metavolcanic sequences, some of which have volcanic arc affinities (Gray, 1986; Wright and Wyld, 1994). The mélange contains fossil-bearing blocks as young as Norian and the entire sequence is cut by plutons as young as ca. 193 Ma (Wright and Wyld, 1994).

The western Hayfork terrane structurally overlies the Rattlesnake Creek terrane along a regional thrust fault. The terrane consists primarily of clastic metasedimentary rocks that range from cobble-rich breccia (lahar deposits) through graded sandstones to fine-grained massive and well-layered argillite. Andesitic and basaltic lavas are uncommon (Irwin, 1972; Wright, 1982). The unit is generally considered to be a clastic apron deposited along the flanks of a volcanic arc. Donato et al.

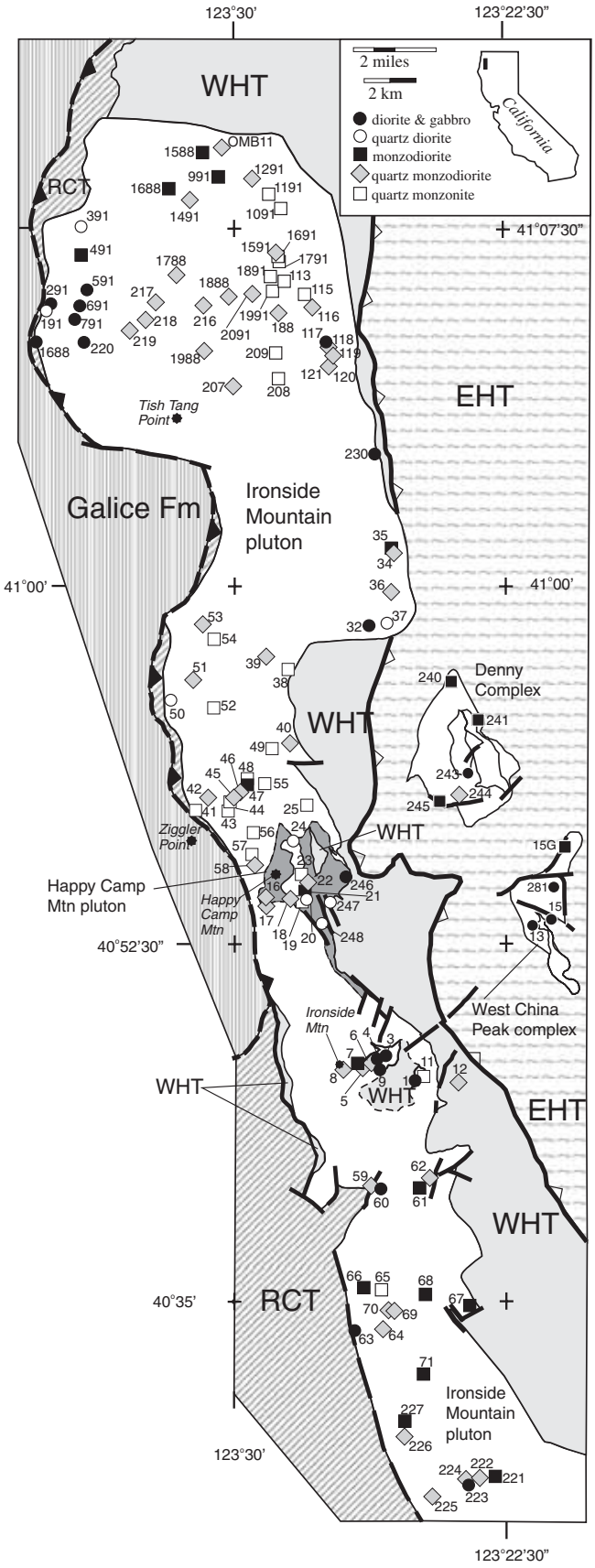

Figure 1. Simplified geologic map of the Ironside Mountain batholith. Bold lines are faults; unornamented lines are high angle faults; Orleans thrust fault shown with filled barbs; Wilson Point thrust fault shown with open barbs. Numbers adjacent to sample location symbols are sample numbers. EHT—eastern Hayfork terrane, RCT—Rattlesnake Creek terrane, WHT—western Hayfork terrane. Modified after Charlton (1979), Donato et al. (1983), and Mars, (1999).

(1996) showed that, at the latitude of the Oregon-California border, the western Hayfork terrane was deposited on Rattlesnake Creek terrane basement (also see Wright and Fahan, 1988). This stratigraphic link suggests that the thrust fault that separates the Rattlesnake Creek terrane and the western Hayfork terrane is of limited displacement (Wright and Fahan, 1988; Donato et al., 1996). The $^{40}Ar/^{39}Ar$ ages on hornblende (considered to be detrital volcanic hornblende) from the western Hayfork range from 168 ± 1.9 Ma to 173 ± 1 Ma (Wright and Fahan, 1988; Donato et al., 1996), and at least one 174-Ma pluton (Squaw Mountain pluton; U-Pb, zircon; Irwin and Wooden, 1999) intrudes the terrane.

The eastern Hayfork terrane overlies the western Hayfork terrane along the Wilson Point thrust (Wright, 1982; Fig. 1). The eastern Hayfork terrane is a chert-argillite mélange and broken formation; it has yielded late Triassic fossils (Wright, 1982; Ernst, 1998). The timing of displacement on the Wilson Point thrust is uncertain, and Wright and Fahan (1988) suggested that it postdated emplacement of the Ironside Mountain batholith. Below we show that the batholith intruded the Wilson Point thrust and therefore places an important constraint on the age of thrusting.

Magmatism with chemical similarities to the Ironside Mountain batholith ended at ca. 167 Ma with emplacement of the Denny complex (see below). Younger magmatic activity, herein referred to as "Wooley Creek belt" magmatism, began at ca. 165 Ma (Hacker et al., 1995; Allen and Barnes, this volume) and continued to ca. 156 Ma (Yule et al., this volume). Wooley Creek belt plutons are composite; they all display field, geochemical, and isotopic evidence for open-system behavior, such as magma mixing and mingling, in situ assimilation, and deep-seated crustal melting (Barnes et al., 1986, 1990, 1995; Gribble et al., 1990).

Intrusive Units and Definition of the Batholith

Irwin (1960) named the Ironside Mountain batholith for an elongate plutonic mass that extends 72 km from 40°32′N latitude to 41°10′N (Fig. 1). The main part of the Ironside Mountain batholith reaches 12 km wide in its northern part, where it is in intrusive contact with host rocks to the east and west. In his original definition, Irwin (1960) mapped an arm that extended southeast from the center of the main mass; however, this extension was shown by Charlton (1979) to be a separate pluton, the Denny zoned complex (Fig. 1). The U-Pb (zircon) dating of

the Ironside Mountain batholith and Denny Zoned Complex (Wright and Fahan, 1988) yielded ages of 169–170 Ma and 167 Ma, respectively.

Charlton's (1979) detailed study of the central part of the Ironside Mountain batholith identified a number of intrusive units internal and external to the main mass of the batholith. The principal external units are the so-called "concentrically-zoned complexes" at Denny and West China Peak (Fig. 1), both of which are intrusive into the eastern Hayfork terrane. These plutons contain ultramafic to intermediate rocks that range from olivine pyroxenite to quartz diorite.

Within the main outcrop area of the batholith, Charlton defined two principal units. The "Ironside Mountain pluton" is the elongate, dioritic to quartz monzonitic body that underlies most of the batholith (Fig. 1). Charlton (1979) interpreted this part of the batholith to be gradationally zoned from diorite to quartz monzonite (but see below). Charlton (1979) also mapped a sequence of dioritic, quartz dioritic, and tonalitic rocks that underlie an ~8-km^2 part of the pluton (Fig. 1) and small areas east of Ironside Mountain. This "Happy Camp Mountain pluton" is intruded by dikes from the Ironside Mountain pluton but has not been radiometrically dated. Charlton (1979) also mapped a number of small dioritic and gabbroic bodies, some of which have appinitic texture.

Although our mapping suggests that rocks similar to those of the Happy Camp Mountain pluton are unusual elsewhere in the batholith, we retain the terminology introduced by Charlton with slight modification. We consider the "Ironside Mountain batholith" to consist of the Ironside Mountain pluton, as defined by Charlton (1979), the "quartz diorite of Happy Camp Mountain," the "Denny intrusive complex," and the "West China Peak intrusive complex." Definitive inclusion of the latter pluton in the Ironside Mountain batholith awaits radiometric dating. This chapter is primarily on the Ironside Mountain pluton, but data are also presented for the quartz diorite of Happy Camp Mountain, the Denny intrusive complex, and the West China Peak intrusive complex.

Contact Relationships

Most of the contacts between the Ironside Mountain pluton and Rattlesnake Creek terrane are sheared. Contact zones are typically marked by mylonitic or submylonitic fabrics and local development of S-C fabrics. Along the northwestern contact, metaserpentinite of the Rattlesnake Creek terrane is tectonically shuffled into the pluton. In some locations, the plutonic rocks have been rodingitized adjacent to the metaserpentinite. However, in the same region (Mill Creek drainage: ~123°34′W, 41°08′N), the grain size of the pluton decreases from medium- and coarse-grained in the interior to fine-grained within ~50 m of the contact. We interpret this grain size decrease to result from undercooling against Rattlesnake Creek terrane host rocks and therefore conclude that the original intrusive contact was intensely modified by later faulting, possibly during Nevadan-age thrusting.

Contacts between the Ironside Mountain pluton and the western Hayfork terrane are clearly intrusive in many locations. These intrusive relations are most commonly seen as development of pyroxene and hornblende hornfels in the western Hayfork terrane and xenoliths of western Hayfork terrane rocks near Ironside Mountain (Charlton, 1979; Fig. 1). Unusual quartz-rich sandstone of the western Hayfork terrane is in contact with the pluton northwest of the Denny complex (south of sample location 37; Fig. 1). Contact metamorphism of the sandstone resulted in a plagioclase + orthoclase + quartz + biotite + garnet + cordierite assemblage.

The Ironside Mountain pluton is in contact with the eastern Hayfork terrane for ~4 km near 123°25′W and 41°00′N. Along this contact, chert-argillite breccias of the eastern Hayfork terrane are metamorphosed to augite-bearing hornfels, and metaserpentinite blocks in the chert-argillite matrix contain augite neoblasts intergrown with olivine. These contact metamorphic effects overprint subgreenschist- to greenschist-facies regional assemblages (e.g., Wright, 1982) and show that the Ironside Mountain pluton intruded the eastern Hayfork terrane.

In summary, the Ironside Mountain batholith was emplaced into a stack of tectonostratigraphic terranes (Rattlesnake Creek, western Hayfork, and eastern Hayfork) that were juxtaposed prior to 170 Ma. The Ironside Mountain pluton intruded the Wilson Point thrust, and therefore places a minimum age on juxtaposition of the eastern and western Hayfork terranes. This assemblage of thrust slices plus the intrusive rocks of the batholith were thrust over the Galice Formation along the Orleans thrust during the Nevadan orogeny (155–150 Ma; Saleeby et al., 1982; Harper and Wright, 1984; Harper et al., 1994), so that parts of the Ironside Mountain batholith are in direct thrust contact over slates of the Galice Formation (Fig. 1).

PETROGRAPHY

Ironside Mountain Pluton

The principal rock types in the Ironside Mountain pluton range from diorite to quartz monzonite (Fig. 1). In most parts of the pluton, zoning is weak or absent. Charlton (1979) mapped a gradational contact in the Ironside Mountain area between western diorite and monzodiorite and eastern quartz monzonite; however, he did not give sample locations, so it is impossible to represent his modal data in Figure 1. In the northern part of the pluton, a crude gradation exists from predominantly dioritic rocks in the west through quartz monzodiorite and monzodiorite in the central part and quartz monzonite near the eastern contact (Fig. 1).

Mafic magmatic enclaves are sparse. They range from gabbro and diorite through monzodiorite. Most are fine grained and equigranular; a few have plagioclase phenocrysts as long as 5

mm. Unlike other dioritic plutons in the Klamath Mountains (e.g., Grayback: Barnes et al., 1995; Johnson and Barnes, this volume; Wooley Creek: Barnes, 1983; Bear Mountain: Snoke et al., 1981; Bushey et al., this volume; English Peak: Schmidt, 1994), the Ironside Mountain pluton lacks swarms of mafic magmatic enclaves and abundant synplutonic mafic dikes.

Texture varies little in the pluton and is predominantly hypidiomorphic granular, with euhedral to subhedral pyroxenes and lath-shaped to blocky plagioclase, anhedral biotite, and interstitial quartz. Alkali feldspar habits range from interstitial to poikilitic to blocky. Where present, hornblende is interstitial in the more mafic rocks and becomes progressively more prismatic in evolved compositions.

Gabbro, Diorite, Monzogabbro, and Monzodiorite. These rocks are characterized by augite, orthopyroxene, and commonly by inverted pigeonite (Fig. 2; Table 1). A few samples contain olivine rimmed by a vermicular intergrowth of orthopyroxene and Fe-Ti oxide. Others contain the vermicular intergrowth but lack olivine; such samples are inferred to have had olivine on the liquidus. The sequence of pyroxene crystallization was apparently augite and pigeonite (the two phases show mutual rimming relations) followed by orthopyroxene, which rims inverted pigeonite. In many samples, hornblende is absent and in others, biotite is rimmed by or intergrown with hornblende. Plagioclase ranges from An_{66} to about An_{48} in quartz-free samples and from An_{56} to An_{28} in quartz-bearing ones (Table 2). Apatite and Fe-Ti oxides are common accessory phases.

Quartz Monzodiorite and Quartz Diorite. These rocks show a transition from two- and three-pyroxene mafic assemblages to increasing proportions of biotite and hornblende. Alkali feldspar habits range from poikilitic to blocky, with alkali feldspar crystals euhedral against interstitial quartz. Plagioclase ranges from An_{50} to An_{30} (Table 2). Where it is in contact with alkali feldspar, it shows rounded (resorbed?) contacts. Accessory phases are apatite, Fe-Ti oxides, and typically zircon ± allanite.

Quartz Monzonite, and Syenite. The proportion of biotite and hornblende increases in quartz monzonite, but some samples still preserve three-pyroxene assemblages as inclusions in hornblende. More commonly, the pyroxenes are altered to actinolitic amphibole and cummingtonite. Plagioclase ranges from An_{45} to An_{22}. An unusual hornblende-bearing pyroxene syenite dike (92OMB116C) contains plagioclase that ranges from An_{64} to An_{14}; most crystals range from An_{47} to An_{28}. Some samples contain alkali feldspar phenocrysts as long as 2 cm, and poikilitic alkali feldspar with euhedral faces against quartz is also present. Accessory phases are the same as for quartz monzonite.

The sequence of crystallization, as inferred from rimming and possible reaction relations, is shown in Figure 3. Olivine appeared first, followed by augite and plagioclase. We infer augite stability before pigeonite because cumulate olivine pyroxenites in the batholith contain augite but lack pigeonite (see below). Hornblende stability is shown with a dashed line because it is absent in many samples. Likewise, we infer the plagioclase in quartz monzodiorite and quartz monzonite was not a solidus phase but was in reaction with the interstitial melt (e.g., Nekvasil and Lindsley, 1990).

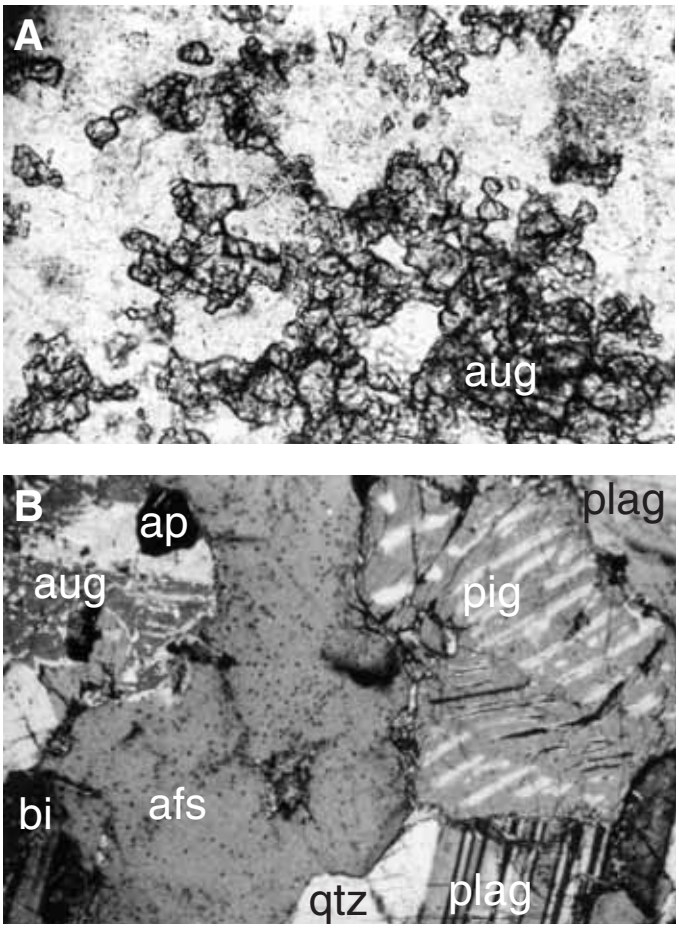

Figure 2. (A) Photomicrograph of pyroxene hornfels from the contact of the Ironside Mountain pluton and chert-argillite breccia of the eastern Hayfork terrane, sample 93OMB234. Field of view is 0.5 mm. (B) Photomicrograph of quartz-bearing biotite, three-pyroxene monzogabbro (sample OMB1688) showing augite (aug), inverted pigeonite (pig), plagioclase (plag), poikilitic orthoclase (afs), and interstitial biotite (bi) and quartz (qtz). The augite is intergrown with prismatic apatite (ap). Field of view is 1.8 mm.

Quartz Diorite of Happy Camp Mountain

This unit is typically medium-grained and hypidiomorphic granular. Augite and orthopyroxene are partly rimmed by olive to pale-green hornblende; brown biotite is interstitial. Lath-shaped to blocky plagioclase ranges from An_{51} to An_{36} (Table 2), and alkali feldspar is interstitial to blocky. The accessory phases are zircon, apatite, and minor Fe-Ti oxides.

TABLE 1. SAMPLE LOCATIONS AND ROCK TYPES

Sample	N latitude (° ′ ″)	W longitude (° ′ ″)	Rock type
Ironside Mountain pluton			
OMB11A	41 09 13.2	123 30 18.3	Biotite-bearing pyroxene monzodiorite
OMB11B	41 09 13.2	123 30 18.3	Dioritic dike
OMB1588A	41 09 06.4	123 30 50.2	Quartz- and biotite-bearing three-pyroxene monzodiorite
OMB1588B	41 09 06.4	123 30 50.2	Biotite-bearing three-pyroxene monzodiorite; mafic enclave
OMB1588C	41 09 06.4	123 30 50.2	Biotite-bearing three-pyroxene gabbro; mafic enclave
OMB1688	41 08 21.2	123 31 45.6	Quartz-bearing biotite three-pyroxene monzogabbro
OMB1788	41 06 31.7	123 34 14.0	Biotite three-pyroxene quartz monzodiorite
OMB1888	41 06 03.9	123 30 10.5	Biotite hornblende three-pyroxene quartz monzodiorite
OMB1988	41 04 56.0	123 30 50.7	Biotite three-pyroxene quartz monzodiorite
OMB491	41 06 55.1	123 34 14.0	Biotite three-pyroxene monzodiorite
OMB791	41 06 35.3	123 34 26.6	Altered biotite hornblende two-pyroxene diorite
OMB991	41 08 36.3	123 30 23.0	Quartz-bearing biotite three-pyroxene monzodiorite
OMB1191	41 08 13.3	123 29 00.5	Biotite hornblende three-pyroxene quartz monzonite
OMB1391	41 08 37.1	123 29 47.4	Hornblende lamprophyre dike
OMB1491	41 08 06.9	123 31 11.6	Biotite three-pyroxene quartz monzodiorite
OMB1591A	41 07 00.1	123 28 52.1	Biotite hornblende three-pyroxene quartz monzodiorite
OMB1591B	41 07 00.1	123 28 52.1	Three-pyroxene quartz monzodiorite
OMB1691	41 06 54.6	123 28 48.4	Biotite granite dike
OMB1891	41 06 29.3	123 28 59.4	Biotite hornblende two-pyroxene quartz monzonite
OMB2091	41.06 07.7	123 29 31.8	Olivine- and biotite-bearing gabbronorite
92OMB1	40 49 39.4	123 24 57.9	Augite hornblende appinite
92OMB3	40 50 08.3	123 25 50.5	Quartz-bearing biotite two-pyroxene diorite
92OMB4	40 50 04.7	123 26 03.5	Hornblende diorite
92OMB5	40 50 01.0	123 26 08.8	Hornblende-bearing biotite two-pyroxene quartz monzodiorite
92OMB7	40 50 04.7	123 26 32.7	Two-pyroxene diorite; mafic enclave
92OMB11	40 49 43.0	123 24 43.3	Two-pyroxene hornblende quartz monzodiorite
92OMB12	40 49 46.5	123 23 51.3	Augite hornblende quartz monzodiorite
92OMB22	40 53 35.5	123 27 58.6	Biotite two-pyroxene hornblende quartz monzodiorite
92OMB23	40 53 57.7	123 28 05.4	Biotite hornblende quartz monzodiorite
92OMB25	40 55 25.4	123 27 56.0	Pyroxene- and biotite-bearing hornblende quartz monzonite
92OMB32	40 58 54.5	123 25 56.3	Quartz- and K-feldspar-bearing hornblende biotite diorite
92OMB35	41 00 47.2	123 25 35.5	Biotite- and quartz-bearing hornblende three-pyroxene monzonite
92OMB36	40 59 53.7	123 25 35.4	Biotite hornblende granite
92OMB38	40 58 16.0	123 28 27.3	Augite-bearing biotite hornblende quartz monzonite
92OMB39	40 58 31.9	123 29 02.7	Biotite-bearing hornblende quartz monzodiorite
92OMB40	40 56 43.2	123 28 25.2	Biotite hornblende quartz monzodiorite
92OMB43	40 55 18.7	123 30 05.9	Biotite- and pyroxene-bearing hornblende quartz monzonite
92OMB44	40 55 30.2	123 30 05.2	Biotite-bearing pyroxene quartz monzonite
92OMB54	40 58 54.5	123 30 32.8	Biotite two-pyroxene hornblende quartz monzonite
92OMB55	40 55 50.4	123 29 04.8	Biotite two-pyroxene hornblende quartz monzonite
92OMB57	40 54 22.3	123 29 25.6	Biotite hornblende quartz monzonite
92OMB58	40 54 08.4	123 29 20.9	Hornblende biotite two-pyroxene quartz monzodiorite
92OMB61	40 47 23.7	123 24 49.6	Biotite-bearing pyroxene monzodiorite
92OMB67	40 44 54.9	123 23 25.7	Biotite hornblende two-pyroxene monzodiorite
92OMB70	40 44 48.5	123 25 38.0	Hornblende biotite granodiorite dike
92OMB113	41 06 23.5	123 28 39.0	Quartz-bearing two-pyroxene hornblende monzonite
92OMB207	41 04 10.8	123 30 01.0	Quartz-bearing biotite three-pyroxene monzodiorite
92OMB116A	41 05 51	123 27 48	Biotite two-pyroxene hornblende quartz monzodiorite
92OMB117	41 05 08	123 27 27	Biotite three-pyroxene diorite; mafic enclave
92OMB118	41 05 06	123 27 25	Biotite two-pyroxene quartz monzodiorite
92OMB121	41 04 37	123 27 21	Quartz-bearing biotite three-pyroxene monzodiorite
92OMB188	41 06 08	123 28 44	Biotite two-pyroxene quartz monzodiorite
92OMB220A	41 05 06	123 24 11	Olivine pyroxenite
92OMB220B	41 05 06	123 24 11	Gabbronorite
93OMB224	40 41 16	123 23 35	Biotite hornblende quartz monzodiorite
93OMB227	40 42 29	123 25 12	Biotite- and quartz-bearing two-pyroxene monzodiorite
Quartz diorite of Happy Camp Mountain			
92OMB19	40 53 22 8	123 28 04.9	Pyroxene-bearing biotite hornblende quartz monzonite
92OMB24	40 54 39.0	123 28 17.4	Biotite augite hornblende quartz diorite
93OMB247	40 53 22	123 26 50	Biotite two-pyroxene quartz diorite

TABLE 1. *Continued*

Sample	N latitude (° ′ ″)	W longitude (° ′ ″)	Rock type
West China Peak complex			
92OMB13	40 52 53	123 21 41	Quartz-bearing biotite augite diorite
92OMB14A	40 53 12	123 21 06	Olivine pyroxenite
92OMB15	40 53 02	123 21 09	Quartz-bearing hornblende biotite two-pyroxene diorite
92OMB15G	40 54 34	123 20 53	Biotite hornblende augite monzodiorite
Denny complex			
93OMB244	40 55 38	123 23 47	Hornblende biotite two-pyroxene quartz diorite
93OMB245	40 55 30	123 24 20	Two-pyroxene hornblende diorite

TABLE 2. RANGE OF PLAGIOCLASE COMPOSITIONS AND AVERAGE ALKALI FELDSPAR COMPOSITIONS

	Plagioclase maximum and minimum An			K-feldspar average composition (standard deviation)		
Sample	An	Ab	Or	An	Ab	Or
Ironside Mountain pluton						
OMB1688. Biotite three-pyroxene quartz-bearing monzodiorite						
max An	46.5	51.7	1.8	1.8	14.3	82.5
min An	27.2	70.1	2.7	(3.7)	(8.0)	(11.2)
OMB491. Biotite three-pyroxene monzodiorite						
max An	65.8	32.6	1.6			
min An	50.9	47.0	2.0			
OMB991. Biotite three-pyroxene quartz-bearing monzodiorite						
max An	55.7	42.9	1.4	2.9	17.2	78.7
min An	32.6	66.5	0.9	(4.4)	(7.5)	(11.5)
OMB1191. Biotite amphibole three-pyroxene quartz monzodiorite						
max An	48.7	50.0	1.3	1.6	15.1	82.6
min An	29.4	69.2	1.4	(3.5)	(9.4)	(12.4)
92.OMB116C. Pyroxene syenite						
max An	63.9	35.8	0.4	1.7	16.7	81.0
min An	14.2	83.6	2.3	(2.8)	(9.6)	(11.7)
93OMB221C. Biotite-bearing orthopyroxene augite monzodiorite						
max An	58.1	39.8	2.1	3.2	13.6	81.7
min An	47.7	49.6	2.8	(5.5)	(3.5)	(8.4)
93OMB224. Biotite amphibole quartz monzodiorite						
max An	45.1	53.5	1.4	0.5	15.9	82.1
min An	22.3	76.6	1.1	(0.7)	(4.9)	(5.4)
Quartz diorite of Happy Camp Mountain						
93OMB248. Biotite orthopyroxene augite diorite						
max An	50.9	47.6	1.5			
min An	35.8	62.8	1.5			
Denny complex						
93OMB242. Plagioclase-bearing olivine amphibole clinopyroxenite						
Average An	88.8	11.0	0.1			
93OMB243. Gabbronorite						
max An	72.9	26.6	0.6			
min An	50.0	48.7	1.3			
West China Peak dike in eastern Hayfork terrane						
93OMB278. Amphibolte augite diorite						
max An	88.90	10.89	0.21			
min An	25.05	73.83	1.12			

Notes: Ab = Na/(Ca + Na + K); An = Ca/(Ca + Na + K); Or = K/(Ca + Na + K).

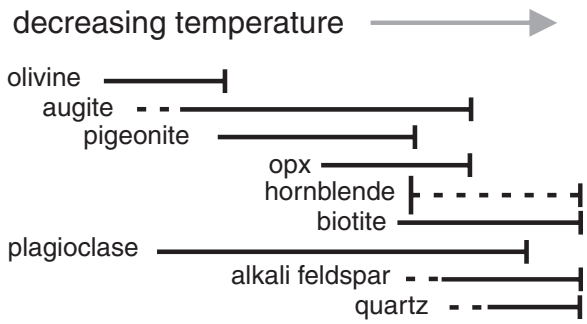

Figure 3. Inferred sequence of crystallization. Solid lines indicate mineral stability in all samples; broken lines indicate minerals present in some samples.

Denny Intrusive Complex

Pyroxenite in the Denny intrusive complex is medium to coarse grained, with subhedral to anhedral olivine (Fo_{72}; Table 3), subhedral augite, and interstitial calcic plagioclase (An_{88}; Table 2). Olivine and plagioclase are compositionally uniform within 1 mole %. Minor element concentrations in olivine (CaO, NiO, and MnO) are less than 0.06, 0.11, and 0.48, respectively. The remainder of the intrusion is predominantly gabbroic to quartz dioritic, with variable proportions of augite, orthopyroxene, hornblende, and biotite. Plagioclase from sample 93OMB243, an opx augite gabbro, is as calcic as An_{73}, and most plagioclase is more calcic than An_{60}; rim compositions are as sodic as An_{48} (Table 2). When compared to the Ironside Mountain pluton, the dioritic rocks of the Denny complex are distinct in their relative abundance of hornblende, the lack of inverted pigeonite, and lower abundances of alkali feldspar and Fe-Ti oxides.

West China Peak Intrusive Complex

Pyroxenite in the West China Peak intrusive complex is similar to that in the Denny intrusive complex. Olivine is slightly more magnesian than that in the Denny complex (Fo_{83} to Fo_{78}; Table 3), but is otherwise similar in composition. The remaining samples range from gabbro to monzodiorite; they are petrographically similar to dioritic and monzodioritic rocks of the Ironside Mountain pluton, including the presence of relict olivine in gabbroic and dioritic samples. A fine-grained hornblende augite gabbro dike adjacent to the West China Peak complex has plagioclase with An_{89} to An_{73} cores and An_{28} to An_{25} rims.

Mineral Compositions

The ranges of plagioclase compositions are given above for each rock type and in Table 2. Compositions of alkali feldspar and the mafic silicates are presented here.

Alkali Feldspar. Poikilitic and phenocrystic alkali feldspar is typically microperthitic and lacks polysynthetic twins. Average compositions were calculated from multiple line traverses across oikocrysts or phenocrysts (Table 2). Although the num-

TABLE 3. SUMMARY OF OLIVINE AND PYROXENE COMPOSITIONS

	Olivine	Clinopyroxene				Orthopyroxene			
Sample	Mg#	Mg#	Mg	Fe	Ca	Mg#	Mg	Fe	Ca
Ironside Mountain pluton									
OMB1688		0.638	0.358	0.203	0.439	0.522	0.509	0.467	0.024
OMB491		0.640	0.363	0.204	0.433	0.532	0.52	0.458	0.023
OMB991		0.621	0.351	0.214	0.436	0.492	0.479	0.494	0.028
OMB1191		0.579	0.323	0.235	0.443	0.437	0.424	0.546	0.03
92OMB116C		0.576	0.326	0.24	0.435	0.465	0.445	0.517	0.033
93OMB221		0.656	0.37	0.194	0.436				
Quartz diorite of Happy Camp Mountain									
93OMB248		0.633	0.351	0.203	0.446	0.482	0.471	0.505	0.024
Denny complex									
93OMB242	0.70–0.72	0.843	0.46	0.086	0.454				
93OMB243		0.754	0.424	0.139	0.437	0.615	0.601	0.376	0.022
West China Peak complex									
93OMB278		0.765	0.43	0.133	0.438				
93OMB280	0.79–0.82	0.864	0.463	0.073	0.464				

Note: Mg# = Mg/(Mg + Fe).

ber of points used to calculate these averages ranges from 24 to 129, standard deviations are still large. Despite these large standard deviations, the average compositions of alkali feldspars from a range of Ironside Mountain pluton rocks types (monzogabbro to syenite) are quite similar, with molar Or from 78.7 to 82.6, Ab from 14.3 to 17.2, and An from 0.5 to 3.2.

Pyroxene. All pyroxenes analyzed during this study are exsolved. In the Ironside Mountain pluton, augite contains orthopyroxene lamellae parallel to (001) and (010), which indicates exsolution of pigeonite followed by orthopyroxene. Inverted pigeonite contains augite lamellae parallel to (001) and (010), whereas primary orthopyroxene contains augite lamellae parallel to (010). In contrast, augite from the Denny and West China Peak complexes contains exsolution lamellae of orthopyroxene parallel to (010); orthopyroxene from the Denny complex exsolved augite on (010).

Because of the complex exsolution among pyroxenes in the batholith, detailed reconstruction of primary pyroxene compositions has not yet been undertaken. Initial compositional data of exsolved samples show lower values of Mg/(Mg + Fe) in the Ironside Mountain pluton compared to the Denny and West China Peak complexes (Table 3). For example, the Mg/(Mg + Fe) ratio in augite from the Ironside Mountain pluton ranges from 0.66 to 0.58. Augite in Denny and West China Peak gabbros and pyroxenites has Mg/(Mg + Fe) of 0.75–0.77 and 0.84–0.86, respectively. Orthopyroxene in the Ironside Mountain pluton ranges in Mg/(Mg + Fe) from 0.52 to 0.42, whereas orthopyroxene in Denny complex gabbro has Mg/(Mg + Fe) of 0.62.

Amphibole. Amphibole was analyzed from three samples of the Ironside Mountain pluton (Table 4). The amphibole shows a limited compositional range, with Mg/(Mg + Fe) from 0.47 to 0.36. Calcium (cations per formula unit) ranges from 1.9 to 1.7, Ti from 0.25 to 0.08, and total alkali content from 0.78 to 0.35 (most values >0.55). With few exceptions, Al content ranges from 1.67 to 1.42 per formula unit. According to the classification of Leake et al. (1997), these amphiboles straddle the boundary between ferropargasite and ferro-edenite (Fig. 4). Amphi-

TABLE 4. REPRESENTATIVE AMPHIBOLE AND BIOTITE ANALYSES

	Amphibole						Biotite					
	Ironside Mountain pluton		Denny Complex		West China Peak		Ironside Mountain pluton				HCM	WCP
	OMB	OMB	93OMB	93OMB	93OMB	93OMB	OMB	OMB	OMB	OMB	93OMB	93OMB
Sample	1191	991	224	243	278	278	1688	491	991	1191	248	278
SiO_2	42.19	43.85	42.79	43.65	45.56	45.44	36.51	35.93	36.19	35.77	35.63	35.25
Al_2O_3	9.10	8.59	8.56	9.89	7.80	7.88	13.25	13.94	13.68	13.66	14.61	15.64
FeO	22.56	20.42	23.52	15.84	20.64	19.06	22.31	21.58	22.65	25.08	22.19	22.77
MgO	8.01	9.84	7.50	11.63	10.29	10.75	10.97	10.00	10.76	8.19	11.30	9.58
TiO_2	2.03	1.31	1.72	2.59	1.39	1.47	4.05	5.39	3.59	4.99	3.66	3.39
Cr_2O_3	0.00	0.00	0.00	0.03	0.00	0.02	0.01	0.03	0.00	0.00	0.03	0.00
MnO	0.39	0.33	0.70	0.22	0.42	0.37	0.17	0.07	0.11	0.22	0.19	0.19
CaO	12.14	11.96	10.59	11.23	10.86	10.86	0.00	0.00	0.00	0.03	0.09	0.00
Na_2O	1.55	1.46	1.47	1.56	1.24	1.38	0.04	0.02	0.13	0.19	0.02	0.07
K_2O	1.43	1.27	1.10	0.86	0.84	0.81	9.68	9.65	9.87	9.34	8.33	9.27
Cl	0.68	0.57	0.29	0.00	0.16	0.03	0.58	0.54	0.56	0.39	0.09	0.05
F	0.15	0.22	0.00	0.00	0.00	0.00	0.68	0.23	0.50	0.19	0.00	0.00
Total	100.03	99.58	98.15	97.49	99.17	98.04	97.84	97.15	97.72	97.88	96.11	96.21
	Cations per 23 oxygens						Cations per 22 oxygens					
Si	6.396	6.567	6.619	6.537	6.821	6.837	5.710	5.680	5.701	5.714	5.700	5.677
Al	1.627	1.517	1.560	1.747	1.377	1.397	2.443	2.598	2.541	2.571	2.754	2.968
Fe^{2+}	2.860	2.558	3.042	1.983	2.584	2.398	2.918	2.853	2.984	3.350	2.969	3.067
Mg	1.810	2.197	1.729	2.596	2.297	2.412	2.557	2.356	2.526	1.949	2.695	2.301
Ti	0.231	0.147	0.200	0.292	0.157	0.166	0.477	0.641	0.426	0.599	0.440	0.411
Cr	0.000	0.000	0.000	0.003	0.000	0.003	0.001	0.004	0.000	0.000	0.003	0.000
Mn	0.050	0.042	0.092	0.027	0.054	0.047	0.023	0.009	0.015	0.030	0.026	0.026
Ca	1.972	1.919	1.756	1.802	1.742	1.751	0.000	0.000	0.000	0.005	0.016	0.000
Na	0.457	0.423	0.440	0.453	0.360	0.402	0.013	0.007	0.040	0.060	0.008	0.023
K	0.277	0.242	0.216	0.164	0.161	0.155	1.931	1.946	1.984	1.904	1.699	1.905
Cl	0.174	0.144	0.075	0.001	0.041	0.008	0.154	0.143	0.148	0.107	0.025	0.014
F	0.074	0.105	0.000	0.000	0.000	0.000	0.337	0.117	0.251	0.097	0.000	0.000
Total	15.927	15.860	15.730	15.605	15.594	15.575	16.563	16.354	16.615	16.384	16.335	16.392
Mg#	0.388	0.462	0.362	0.567	0.471	0.501	0.467	0.452	0.458	0.368	0.476	0.429

Notes: HCM—quartz diorite of Happy Camp Mountain, WCP—West China Peak complex, Mg# = Mg/(Mg + Fe).

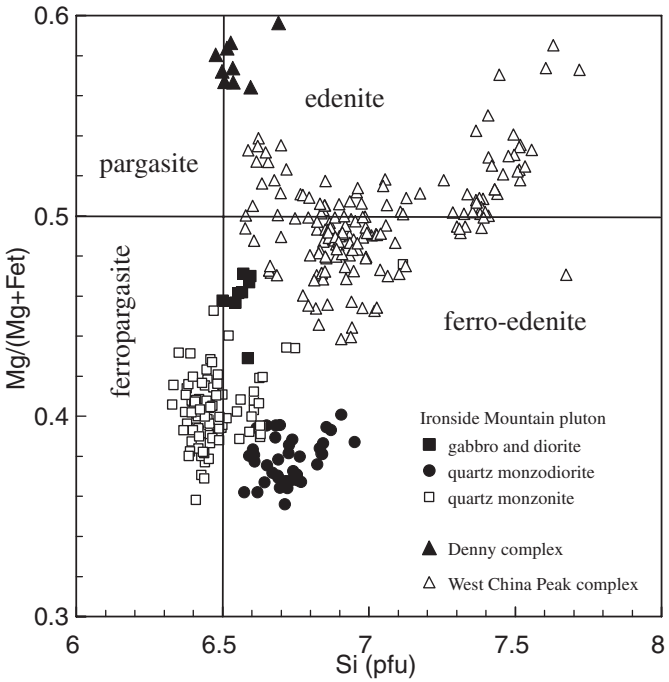

Figure 4. Amphibole classification. Fet indicates total Fe.

bole in a two-pyroxene gabbro from the Denny complex is edenitic (Fig. 4), and amphibole from a biotite hornblende quartz monzodiorite of the West China Peak complex is edenitic to ferro-edenitic. The fluorine content of Ironside Mountain pluton amphibole reaches 0.57 wt% and Cl contents reach 0.25 wt%. Halogen concentrations are below detection limits in amphiboles from other plutons in the batholith.

Biotite. As is typical of many plutonic rocks, biotite from individual samples of the Ironside Mountain pluton is homogeneous. It is characterized by relatively low Mg/(Mg + Fe) (Table 4): from 0.51 (monzogabbro) to 0.35 (quartz monzonite). The Ironside Mountain biotites also contain moderate halogen contents, with F from 0.21 to 0.58 wt% and Cl from 0.40 to 0.57 wt%. There is no obvious correlation between bulk composition and halogen content, although biotite from the most mafic samples shows the highest F and Cl contents. Biotite from the quartz diorite of Happy Camp Mountain has Mg/(Mg + Fe) of 0.47, similar to that of Ironside Mountain pluton samples, but has halogen contents at or below detection limits. Biotite from a West China Peak gabbro has similar Mg/(Mg + Fe) of 0.43 and undetectable halogen contents.

Estimates of P and H_2O Content

Hammarstrom and Zen (1986) and Hollister et al. (1987) showed that for samples with the assemblage calcic amphibole + plagioclase + biotite + K-feldspar + quartz + Fe-Ti oxide + titanite, the total Al content of amphibole crystallized near the solidus is a function of total pressure. Amphibole was analyzed from three samples of the Ironside Mountain pluton. All three samples contain the required mineral assemblage except for titanite, and all show petrographic features that suggest amphibole was stable at the solidus. The lack of titanite should not affect pressure estimates, because Ti content in the melt was buffered by ilmenite (e.g., Anderson and Smith, 1995). The calibration of Schmidt (1992) results in average pressure estimates of 4.1 ± 0.4, 4.4 ± 0.4, and 4.2 ± 0.2 kb for quartz monzonite, quartz monzodiorite, and quartz-bearing monzodiorite, respectively. These estimates are consistent with the presence of contact metamorphic cordierite + garnet in the aureole.

The highest An content in plagioclase from the Ironside Mountain pluton is in the An_{66} range. In contrast, intercumulus plagioclase in hornblende clinopyroxenite from the Denny complex reaches An_{88}. Gabbroic rocks from the Denny and West China Peak complexes have An_{73} and An_{89} plagioclase, respectively. Experimental data (Beard, 1986; Sisson and Grove, 1993) show that plagioclase crystallized from H_2O-rich magmas is calcic relative to plagioclase from similar, but H_2O-poor magmas. These data are consistent with the paucity of hydrous mafic minerals in the Ironside Mountain pluton compared to the Denny and West China Peak complexes, and they emphasize the H_2O-poor nature of the Ironside Mountain pluton.

GEOCHEMISTRY

Major and Trace Elements

Major element compositions of samples from the Ironside Mountain batholith are presented in Table 5 and illustrated in Figure 5. Data from Lanphere et al. (1968), Hotz (1971) and Charlton (1979) are also plotted. These plots are scaled to emphasize the trends of the main part of the batholith; thus, a fine-grained biotite granite dike from the northern part of the Ironside Mountain pluton (sample OMB1691; Table 5) is only plotted in Figure 5A–C, and olivine pyroxenites from the Denny and West China Peak intrusive complexes are not plotted. All but one sample from the Denny and West China Peak intrusive complexes contain less than 54 wt% SiO_2; the sample with higher SiO_2

Figure 5. Major element variation and geochemical classifications. (A) K_2O vs. SiO_2. Boundary lines from Le Maitre et al. (2002) and Rickwood (1989). Shaded field shows the range of compositions from the 165- to 156-Ma Wooley Creek belt plutons. (B) FeO/(FeO + MgO) vs. SiO_2, where FeO is total iron. Boundary between ferroan and magnesian fields from Frost et al. (2001). Shaded field shows the range of compositions from the 165- to 156-Ma Wooley Creek belt plutons; few compositions plot in the ferroan field. (C) Modified alkali-lime index versus SiO_2. See Frost et al. (2001). (D) TiO_2 vs. SiO_2. (E) CaO vs. SiO_2. Shaded field shows the range of compositions from the 165- to 156-Ma Wooley Creek belt plutons. (F) Na_2O vs. SiO_2. Data points outlined are central zone samples enriched in Na_2O and Sr relative to the rest of the Ironside Mountain pluton.

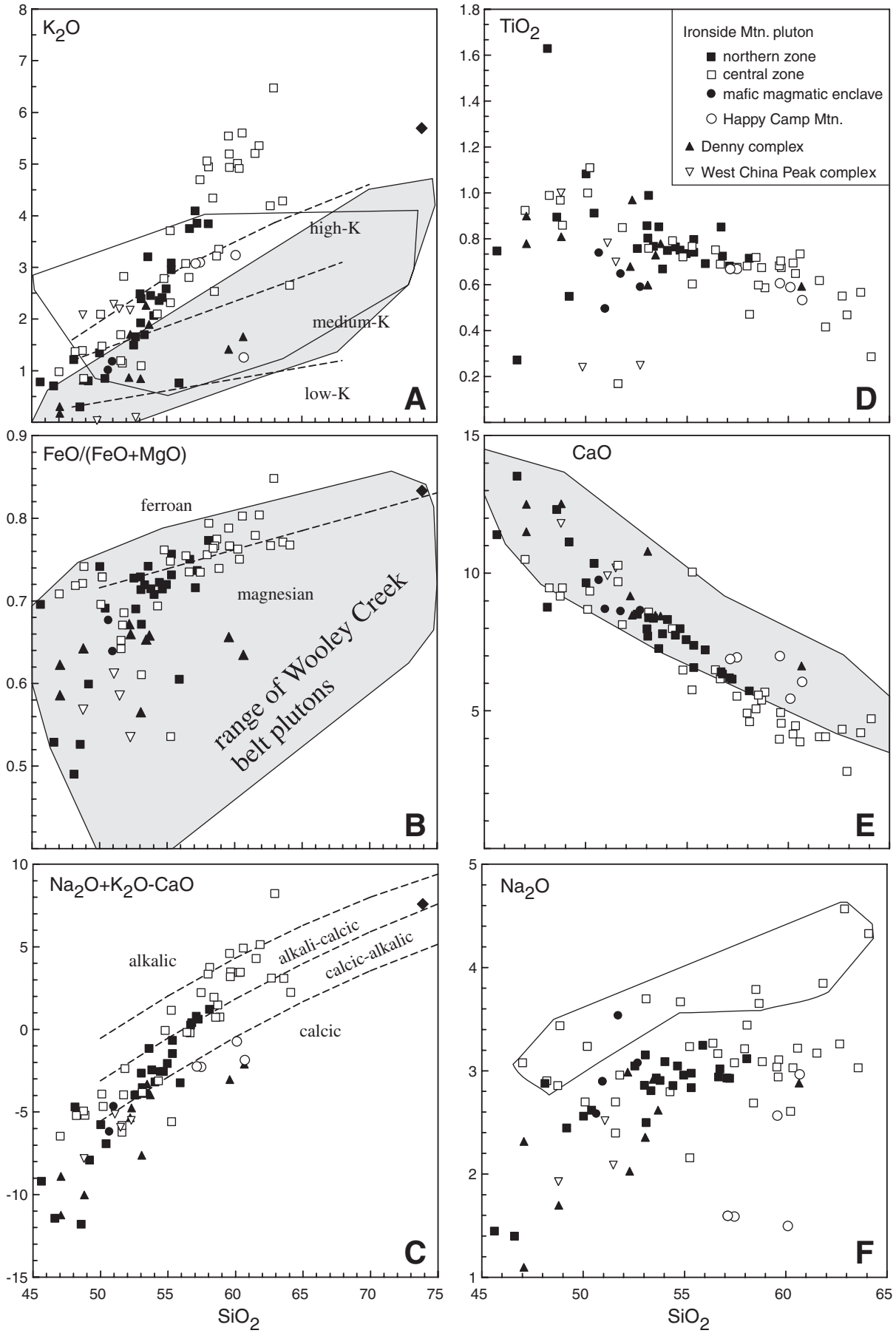

TABLE 5. REPRESENTATIVE MAJOR AND TRACE ELEMENT CONCENTRATIONS

	OMB 1588A	OMB 1588B	OMB 1688	OMB 1788	OMB 1888	OMB 491	OMB 991	OMB 1191	OMB 1491	OMB 1591A	OMB 1591B	OMB 1691
						Ironside Mountain pluton						
Major oxide concentrations (wt%)												
SiO_2	54.96	52.68	54.65	53.80	56.75	50.42	55.33	58.08	53.35	55.33	52.55	73.89
TiO_2	0.74	0.59	0.75	0.67	0.73	0.91	0.74	0.72	0.77	0.80	0.76	0.12
Al_2O_3	16.94	17.44	17.17	17.32	16.19	17.72	16.70	15.95	16.38	16.08	16.31	14.10
Fe_2O_3	2.60	2.04	2.61	3.01	1.97	2.69	1.79	2.10	3.64	2.23	2.72	0.13
FeO	6.72	7.65	6.99	6.25	6.64	8.12	7.26	6.57	6.95	6.99	8.05	1.09
MnO	0.18	0.22	0.20	0.19	0.18	0.20	0.19	0.17	0.22	0.18	0.25	0.02
MgO	3.52	4.25	3.73	3.57	3.03	4.70	3.25	2.48	3.98	2.89	3.92	0.24
CaO	7.60	8.67	8.00	7.81	6.35	10.37	7.39	5.74	8.38	6.58	8.52	1.07
Na_2O	2.96	3.08	3.05	2.91	3.02	2.62	2.98	3.12	2.81	2.84	3.05	2.97
K_2O	2.59	1.66	2.42	2.46	3.76	0.85	2.96	3.85	1.70	3.09	1.50	5.70
P_2O_5	0.44	0.28	0.41	0.34	0.41	0.13	0.40	0.42	0.50	0.47	0.44	0.05
LOI	1.83	1.73	1.06	1.72	1.31	0.97	0.99	1.35	1.28	1.16	1.39	0.99
Total	101.07	100.29	101.04	100.04	100.33	99.69	99.97	100.54	99.95	98.64	99.46	100.37
$Mg/(Mg + Fe^t)$	0.409	0.444	0.416	0.415	0.391	0.443	0.395	0.343	0.410	0.364	0.400	0.263
Trace element concentrations (ppm)												
Rb	73	47	62	65	104	19	74	106	48	86	36	183
Sr	654	695	699	626	591	580	644	472	640	516	517	377
Zr	87	48	91	41	109	35	142	218	31	141	69	93
Y	27.0	22.6	25.8	27.0	29.2	15.0	27.7	35.8	26.6	33.6	31.8	4.2
Nb	9	4	9	8	9	2	5	11	4	7	3	2
Ba	751	523	747	740	1357	424	1089	923	499	775	404	1427
Sc	24.0	28.8	24.7	25.4	21.2	33.9	25.1	22.0	30.2	26.1	34.8	1.2
V	215	206	227	222	170	380	203	160	285	209	242	11
Cr	16	22	18	15	19	42	36	20	27	13	25	b.d.
Ni	b.d.	b.d.	b.d.	b.d.	b.d.	b.d.	26	23	22	b.d.	b.d.	b.d.
Cu	120	53	57	75	88	60	81	114	174	147	88	7
Zn	94	94	98	96	97	93	86	87	105	94	99	15

Notes: Analyzed by inductively coupled plasma atomic emission spectrometry, Melanie Barnes, analyst. Abbreviations: b.d.—below detection limits, HCM—quartz diorite of Happy Camp Mountain, LOI—loss on ignition, n.d.—not analyzed.

content is quartz diorite. Samples from the quartz diorite of Happy Camp Mountain range from 57.1 to 61.7 wt% SiO_2 and have distinctly lower K_2O contents than most samples of the batholith at similar silica contents (Fig. 5A). The Ironside Mountain pluton ranges from 45.5 to 63.6 wt% SiO_2 (Fig. 5A). In these figures, the pluton is divided into northern and central parts, the boundary of which is arbitrarily placed at ~41°02′. The southern part of the pluton was not sampled.

The batholith is subalkaline according to the criteria of MacDonald and Katsura (1964). More detailed distinctions may be made with the geochemical classification of Frost et al. (2001), which shows that the trend of the Ironside Mountain pluton crosses the boundaries between calcic, calc-alkalic, and alkali-calcic rocks (Fig. 5C). In contrast, the other plutons in the batholith are nearly entirely calcic (Fig. 5C). In the Frost et al. (2001) classification scheme, many samples from the Ironside Mountain pluton plot along the boundary between ferroan and magnesian suites (Fig. 5B) and straddle the calc-alkaline/tholeiitic boundary of Middlemost (1975; not shown). According to the criteria of Miyashiro (1974), the pluton is tholeiitic, and its compositional trend is similar to the pigeonite series defined by Kuno (1968). The quartz diorite of Happy Camp Mountain and the Denny and West China Peak complexes are magnesian according to Frost et al. (2001). In Miyashiro's (1974) classification, the Denny and West China Peak compositions plot across the tholeiite/calc-alkaline boundary, but all samples of the quartz diorite of Happy Camp Mountain plot in the calc-alkaline field.

The range of K_2O contents in the Ironside Mountain pluton, which extends from medium to ultra-high K fields, clearly distinguishes it from other plutons in the province (Fig. 5A; Lanphere et al., 1968; Hotz, 1971; Barnes et al., 1992). At 65% SiO_2, few other plutons in the province contain 3 wt% K_2O and none contain 4 wt% (Barnes et al., 1992, 1995, 1996). The most evolved rocks of the pluton are also distinct from typical Klamath Mountain plutons (as characterized by the late Middle Jurassic plutons of the Wooley Creek belt; Barnes et al., 1992) in their relatively Fe-rich and Ca-poor nature (Fig. 5B and E).

OMB 1981	92OMB 3	92OMB 4	93OMB 221	92OMB 24	93OMB 247	93OMB 244	93OMB 245	93OMB 242	93OMB 280	92OMB 13	92OMB 15
Ironside Mountain pluton			**HCM**			**Denny complex**			**West China Peak**		
57.23	48.86	47.01	50.55	60.69	59.58	60.65	53.07	50.46	51.81	51.07	48.78
0.67	0.86	0.93	0.79	0.53	0.61	0.59	0.60	0.29	0.23	0.78	1.00
15.68	20.07	20.15	17.44	15.59	16.15	16.49	15.09	3.41	2.30	14.97	13.46
2.41	10.29	11.86	11.03	6.28	7.73	6.84	9.40	7.46	7.53	10.62	11.39
6.01	n.d.	n.d.	n.d.	n.d.	n.d.	n.d.	n.d.	n.d.	n.d.	n.d.	n.d.
0.17	0.18	0.21	0.19	0.12	0.14	0.13	0.18	0.16	0.15	0.20	0.21
2.92	3.22	4.39	4.9	3.42	3.64	3.54	6.50	16.81	17.15	6.05	7.78
6.16	9.48	10.51	10.25	6.07	7.00	6.64	10.80	20.72	19.59	9.92	11.81
2.93	3.44	3.08	2.97	2.97	2.57	2.88	2.36	0.24	0.23	2.52	1.93
3.86	0.86	0.98	1.37	1.26	1.42	1.66	0.85	0.04	0.03	2.29	2.09
0.36	0.96	0.51	0.35	0.14	0.24	0.16	0.21	0.01	0.02	0.42	0.73
1.47	1.50	1.57	0.26	2.05	1.45	0.75	0.95	0.68	0.71	0.50	1.12
99.87	99.72	101.20	100.10	99.12	100.52	100.35	100.01	100.28	99.75	99.34	100.09
0.389	0.383	0.423	0.468	0.519	0.483	0.506	0.578	0.817	0.819	0.530	0.575
114	18	17	24	32	34	36	16	b.d.	b.d.	53	58
556	1476	1066	892	437	625	557	594	105	62	736	962
178	17	44	43	103	96	87	46	6	2	70	45
27.2	21.6	34.0	21.7	19.8	21.1	19.0	20.2	11.4	8.4	24.1	29.9
8	3	3	3	6	4	3	2	b.d.	b.d.	5	7
799	820	367	654	639	555	830	436	23	20	688	1093
22.5	17.2	35.8	35.3	19.0	20.4	24.3	38.8	n.d.	103	35.3	35.5
180	180	255	310	164	208	134	265	n.d.	152	234	290
32	17	20	42	72	59	50	148	n.d.	1295	129	228
23	24	b.d.	b.d.	49	b.d.	27	25	n.d.	152	50	48
106	6	45	65	54	89	10	39	n.d.	20	39	115
96	90	88	85	64	91	83	81	n.d.	25	84	92

Like most plutons in the province, Na_2O contents show considerable scatter (Fig. 5F). However, much of the scatter can be resolved by recognition of two groups within the pluton. One group is characterized by higher Na_2O over a range of SiO_2 values; it is outlined in Figure 5F. These samples are also richer in Sr and Al_2O_3. Reasons for this compositional distinction are discussed below.

Variations in selected trace element concentrations are shown in Figure 6. The smaller number of data points compared to Figure 5 is because not all data taken from the literature included trace element values.

The concentration of Rb in the Ironside Mountain pluton shows continuous increase with increasing SiO_2 (Fig. 6A). The Zr and Ba contents also increase (Fig. 6D and E, respectively), but both show considerable scatter, particularly at SiO_2 contents higher than ~55 wt%. Furthermore, many samples with the highest Ba concentrations belong to the group of Na_2O-rich rocks illustrated in Figure 5F. If this group is excluded from the compositional trend, then Ba concentrations increase until SiO_2 concentrations reach ~56 wt%, after which little variation in Ba is observed.

Strontium, V, and Sc (Fig. 6B, C, and F) all decrease with increasing SiO_2, as do TiO_2 (Fig. 5D), P_2O_5, and Zn (not shown). Each element shows broad scatter at SiO_2 contents below ~54 wt%, and most show reasonably well-defined trends at higher silica contents. Although Sr concentrations scatter widely, if the group of Na_2O-rich samples discussed is excluded (data points outlined in Fig. 6B), Sr concentrations clearly decrease at SiO_2 contents above 54 wt%. Except for pyroxene-rich cumulates, Sc contents are less than 40 ppm and decrease among samples with SiO_2 >54 wt%. The element Cr (Table 5) is similarly enriched in the pyroxenites, but otherwise is less abundant than 80 ppm and is not correlated with SiO_2. Zn concentrations reach 120 ppm in some pyroxenites, are in the 90–100 ppm range in dioritic and monzodioritic rocks, and decrease to ~60 ppm in the most evolved samples (Table 5).

Figure 7A shows rare-earth element patterns for dioritic to quartz monzonitic rocks from the northern part of the Ironside

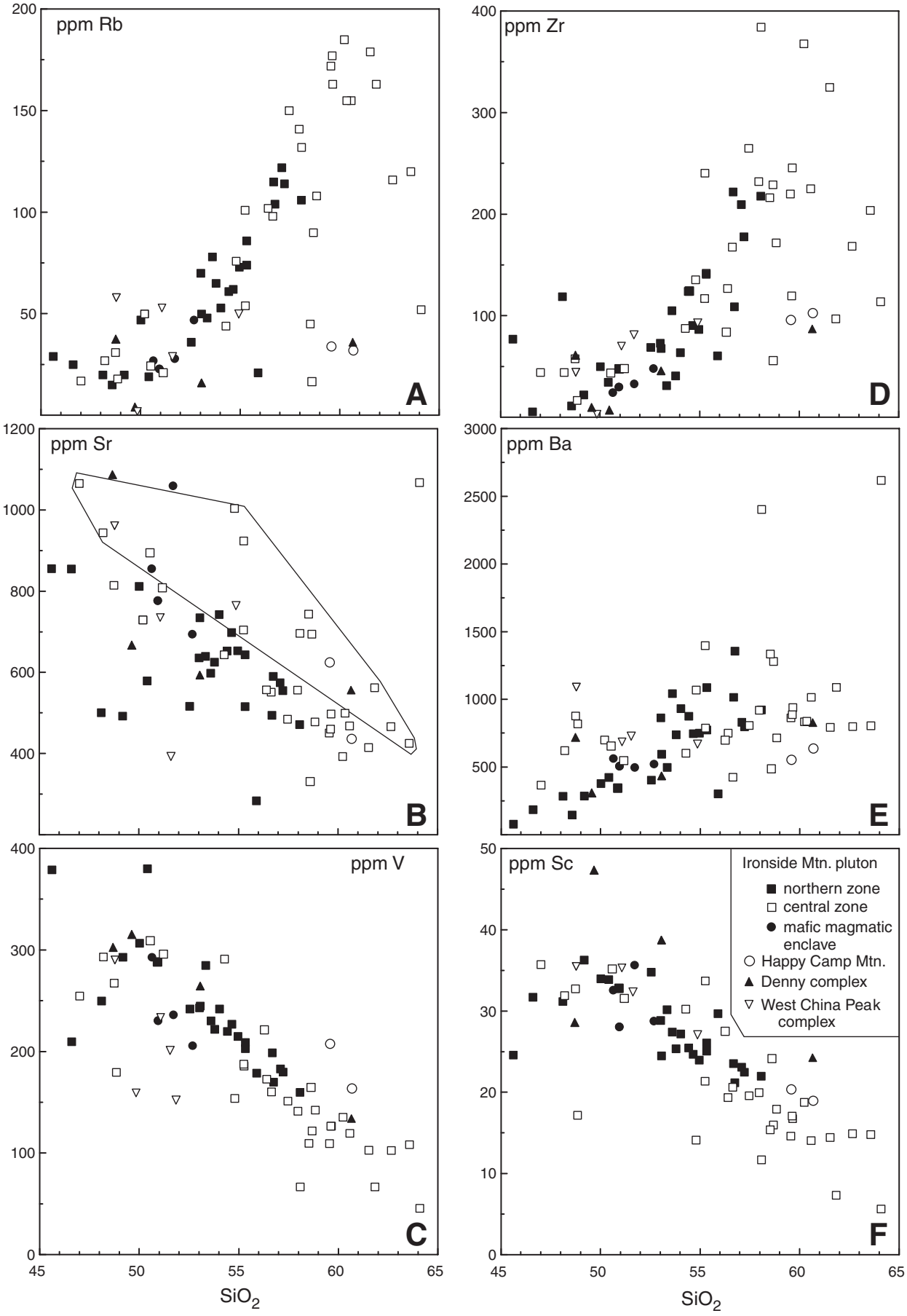

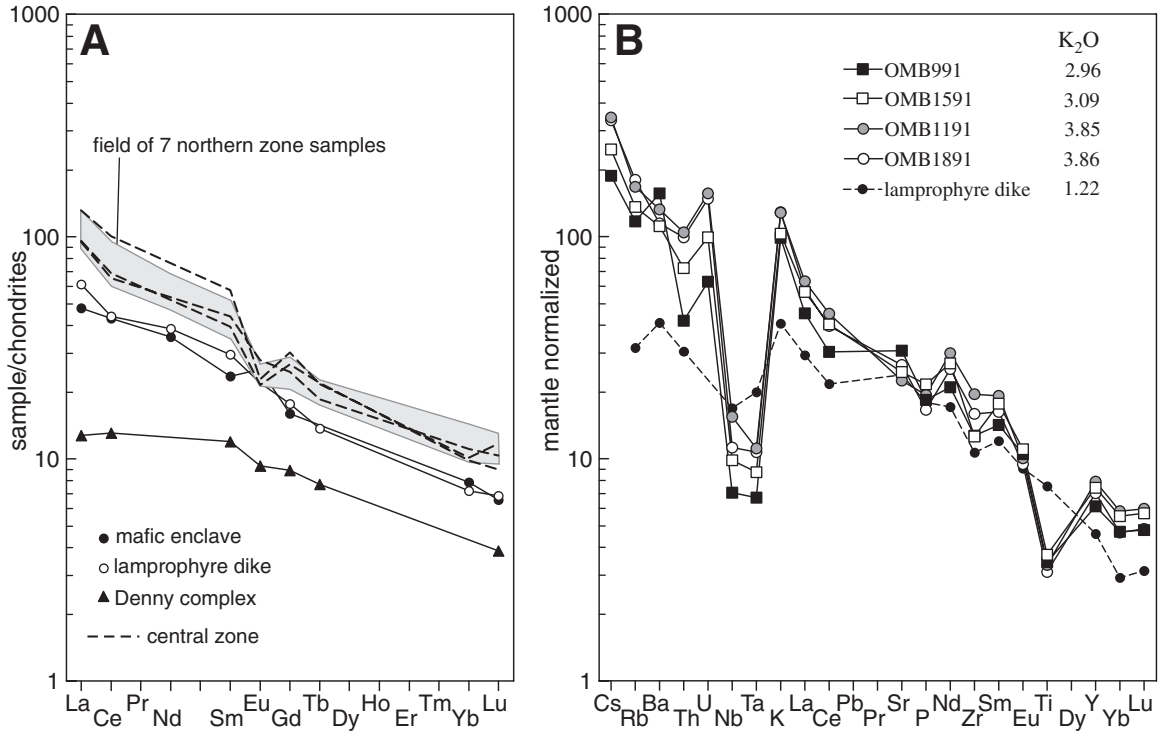

Figure 7. (A) Chondrite-normalized rare-earth element diagrams. The shaded field represents seven samples from the northern zone of the Ironside Mountain pluton; the dashed patterns are for samples from the central part of the pluton. The mafic enclave (OMB1588C) and lamprophyric dike are from the northern zone. (B) Mantle-normalized (Sun and McDonough, 1989) multi-element patterns. The key shows sample numbers and K_2O contents.

Mountain pluton (Table 6). A mafic magmatic enclave (sample OMB1588C) and a hornblende lamprophyre dike (OMB1391) are also plotted. Except for the enclave and dike, the rare-earth element patterns are quite similar, with moderate negative slopes and a negative Eu anomaly. Rare-earth element concentrations broadly increase as a function of increasing SiO_2 (or K_2O). The pattern of the mafic magmatic enclave is similar to that of the host pluton, but with lower rare-earth element abundances and a positive Eu anomaly. The pattern of the lamprophyric dike is similar to the enclave except that the dike sample lacks an Eu anomaly.

The mantle-normalized multi-element diagram (Fig. 7B, Table 6) also shows tightly clustered patterns for four samples of the northern Ironside Mountain pluton. Compared to their neighbor elements, U and K show positive anomalies and Nb, Ta, Ti, and P(?) show negative anomalies. The lamprophyric dike shows similar, but more subdued negative anomalies except for Ti (Fig. 7B).

Figure 6. Trace element variation as a function of SiO_2. In B, data points outlined are central zone samples enriched in Na_2O and Sr relative to the rest of the Ironside Mountain pluton. See text for discussion.

Isotopes

Initial $^{87}Sr/^{86}Sr$ values for eleven samples from the Ironside Mountain pluton (Table 7, calculated at 170 Ma) range from 0.70364 to 0.70397. These data are in agreement with initial $^{87}Sr/^{86}Sr$ values of 0.7036 reported by Masi et al. (1981). One

TABLE 6. TRACE ELEMENT COMPOSITIONS

Sample	OMB991	OMB1191	OMB1591A	OMB1891
La	30.93	43.11	38.53	39.53
Ce	53.55	79.53	71.16	70.15
Nd	28.36	40.4	36.33	34.14
Sm	6.293	8.505	7.825	7.204
Eu	1.76	1.683	1.851	1.589
Tb	0.833	1.051	0.952	0.8407
Yb	2.31	2.86	2.709	2.285
Lu	0.352	0.44	0.42	0.3569
Cs	1.48	2.71	1.94	2.63
Hf	3.53	4.58	3.69	4.05
U	1.31	3.27	2.08	3.1
Th	3.55	8.86	6.12	8.42
Ta	0.273	0.456	0.356	0.439

Notes: Analyses by instrumental neutron activation analysis at the University of Texas, El Paso. Concentrations in ppm.

TABLE 7. Nd AND Sr ISOTOPIC DATA FOR THE IRONSIDE MOUNTAIN BATHOLITH

Sample	Rb (ppm)	Sr (ppm)	$^{87}Rb/^{86}Sr$	$^{87}Sr/^{86}Sr$	Initial $^{87}Sr/^{86}Sr$	Sm (ppm)	Nd (ppm)	$^{147}Sm/^{144}Nd$	$^{143}Nd/^{144}Nd$	Initial $^{143}Nd/^{144}Nd$	Initial ε_{Nd}	Nd model age†
University of Wyoming*												
OMB1491W	32.11	509.37	0.1824	0.70438	0.703935	4.180	19.98	0.12652	0.512820	0.512679	5.08	580 Ma
OMB1788	49.87	543.68	0.2619	0.70444	0.703806	5.700	29.33	0.11753	0.5128245	0.512694	5.36	520 Ma
92OMB39W	93.96	637.20	0.4266	0.70494	0.703905	6.083	33.00	0.11147	0.512815	0.512691	5.30	500 Ma
92OMB13W	40.14	653.19	0.1778	0.70484	0.704412	5.393	27.59	0.11819	0.5127211	0.512590	3.33	690 Ma
U.S. Geological Survey§												
OMB1588A	73.8	644	0.329	0.70444	0.70364							
OMB1588C	34.2	859	0.115	0.70392	0.70364							
OMB1688	63.3	701	0.126	0.70427	0.70397							
OMB1888	97.5	589	0.48	0.70485	0.70369							
OMB1191	104	471	0.639	0.70525	0.70371							
OMB1591B	35.4	541	0.189	0.704213	0.70376							
OMB1691	179	371	1.397	0.707015	0.70364							
OM1891	111	581	0.553	0.705071	0.70373							

*Analytical details: ~80 to 100 mg of sample were dissolved in HF-HNO_3. After conversion to chlorides, one-third of the sample was spiked with ^{87}Rb, ^{84}Sr, ^{149}Sm, and ^{146}Nd. Elements Rb, Sr, and rare-earth elements were separated by conventional cation-exchange procedures; Sm and Nd were further separated in di-ethyl-hexyl orthophosphoric acid colums. All isotopic measurements were made on a VG Sector multi-collector mass spectrometer at the University of Wyoming. An average $^{87}Sr/^{86}Sr$ isotopic ratio of 0.710251 ± 20 (2σ) was measured for NBS 987 Sr, and an average $^{143}Nd/^{144}Nd$ ratio of 0.511846 ± 11 (2σ) was measured for the LaJolla Nd standard. Uncertainties in Sr isotopic ratio measurements are ±0.00002 and uncertainties in Nd isotopic ratio measurements are ±0.00001 (2σ). Blanks are <50 pg for Rb, Sr, Nd, and Sr, and no blank correction was made. Uncertainties in Rb, Sr, Nd, and Sm concentrations are ±2% of the measured value; uncertainties on initial ε_{Nd} = ±0.5 epsilon units. Initial Sr and Nd isotopic ratios and initial ε_{Nd} values are calculated for 170 Ma.

†Nd model ages are calculated based upon the depleted mantle model of Goldstein et al. (1984).

§See Kistler et al. (1986) for analytical details. Analyst: R.W. Kistler.

biotite augite quartz-bearing diorite from the West China Peak intrusive complex has initial $^{87}Sr/^{86}Sr$ (170 Ma) of 0.70441.

Initial ε_{Nd} values were determined for three Ironside Mountain pluton samples (Table 7); they range from 4.2 to 6.1 (calculated at 170 Ma), and the West China Peak diorite has ε_{Nd} of 5.4. Two whole-rock $\delta^{18}O$ values were reported for the Ironside Mountain pluton by Masi et al. (1981); they are 7.7 and 8.8‰.

When compared to isotopic data for slightly younger, but pre-Nevadan Klamath plutons (e.g., Wooley Creek belt plutons; Masi et al., 1981; Barnes et al., 1990, 1992, 1995; Gribble et al., 1990), the Ironside Mountain pluton is characterized by some of the lowest initial $^{87}Sr/^{86}Sr$, highest ε_{Nd}, and lowest $\delta^{18}O$ values. Only a few samples from the Grayback pluton (Barnes et al., 1995) have more primitive isotope values.

DISCUSSION

Compositional Variation in the Ironside Mountain Pluton

Magmatism responsible for the Ironside Mountain batholith is unusual in the Klamath Mountains in a number of ways. First, it occurred shortly after regional thrusting along the Wilson Point thrust. As such, we interpret Ironside Mountain magmatism to mark the beginning of a 15-m.y. episode of magmatic activity that encompassed the Ironside Mountain batholith and related plutons, the large plutons of the Wooley Creek belt, the Josephine ophiolite, and the magmatic arc characterized by the Rogue Formation and the Illinois River gabbro. This episode ended with the onset of Nevadan thrusting at ca. 155 Ma (Harper and Wright, 1984).

Second, relative to typical Klamath magmatism, magmas of the Ironside Mountain pluton evolved toward high K_2O contents and high FeO/(FeO + MgO). In the SiO_2 range of 50–60%, no other plutonic sequence in the province extends to ultra-high K_2O compositions and few (e.g., sparse tholeiitic enclaves and synplutonic dikes in the Grayback pluton: Barnes et al., 1995) have FeO/(FeO + MgO) values greater than 0.7. Furthermore, the most evolved rocks in the pluton have SiO_2 contents of ~64% SiO_2, whereas evolved rocks in the younger plutonic sequences reach 75% SiO_2 (e.g., Barnes et al., 1992, 1996).

Third, unlike nearly all other large Jurassic plutons in the province, the Ironside Mountain pluton lacks significant evidence of magma mixing or mingling. This observation is supported by the lack of reverse zoning of plagioclase, the absence of synplutonic mafic dikes, and the paucity of mafic enclaves.

Mafic rocks in the batholith are also characterized by mafic mineral assemblages indicative of low to very low H_2O contents (e.g., two- or three-pyroxene ± olivine); this assemblage changes gradually to biotite + hornblende in the most evolved rocks (Table 1). Clearly, both biotite and hornblende were only stable late in the crystallization sequence (Fig. 3). Although such assemblages constitute parts of larger plutons in the Wooley Creek belt (e.g., Barnes, 1983; Cotkin and Medaris, 1993) and the Bear Mountain intrusive complex (Snoke et al., 1981; Bushey et al., this volume), the amount of H_2O-poor magma represented by the Ironside Mountain pluton is many orders of magnitude larger.

Another striking characteristic of the Ironside Mountain pluton is the relatively coherent compositional trend. In Figures 5 and 6, this trend encompasses samples collected over an ~50-km-long strike length. Although some hint of zoning is present in the northern part of the pluton (Fig. 1), there is little evidence for compositional zoning elsewhere in the body, except that the most evolved samples were collected in the central part of the pluton. Even so, the central zone contains all of the lithologic types present in the pluton. This lack of obvious zoning could be the result of piecemeal emplacement of numerous magma batches, all of which cooled slowly enough to have similar textural features. This possibility cannot be disproved on geochemical grounds, but it is noteworthy that in areas with good exposure (e.g., east-central parts of the northern zone), internal intrusive contacts were not observed.

If the Ironside Mountain pluton represents magma emplacement over a relatively short time, which is consistent with field relationships, then three simple models may be considered. The first is that compositional variation in the pluton arose via crystal-liquid separation (fractional or equilibrium crystallization), with or without crystal accumulation and magma recharge. The second is that such variation results from variable degrees of partial melting of rather uniform source rocks, and the third is that the variation is the result of variable proportions of mixing between mafic and felsic end members.

The third possibility is unlikely for at least two reasons. First, initial $^{87}Sr/^{86}Sr$ values are uncorrelated with fractionation (e.g., Rb content; Table 7). In fact, the narrow range of initial $^{87}Sr/^{86}Sr$ and ε_{Nd} of the Ironside Mountain pluton is distinct compared to all other large Middle Jurassic plutons in the province, all of which have significant crustal components (e.g., Gribble et al., 1990; Barnes et al., 1992). Second, many binary element plots show curved trends, which is not compatible with simple mixing. In addition, textural and field evidence for mixing (e.g., mantled and disequilibrium crystals; Anderson, 1976) or mingling (e.g., mafic magmatic enclaves) are nearly absent in the pluton.

The first and second possibilities may be tested in binary plots in Figure 8A and B. These diagrams plot the ratio of strongly incompatible element/moderately incompatible element on the *y*-axis against a strongly incompatible element on the *x*-axis (Treuil et al., 1977). For fractional crystallization, the ratio plotted on the *y*-axis shows little variation (near zero slope), whereas for equilibrium partial melting, the ratio has a distinct positive slope. In Figure 8, Rb is used as the "perfectly" incompatible element and Zr and K_2O are used as incompatible elements with slightly larger bulk partition coefficients. The Rb/Zr (Fig. 8A) and Rb/K_2O (Fig. 8B) ratios show little variation; they are not consistent with an origin by partial melting.

We are left with the likelihood that compositional variation in the Ironside Mountain pluton resulted primarily from crystal-

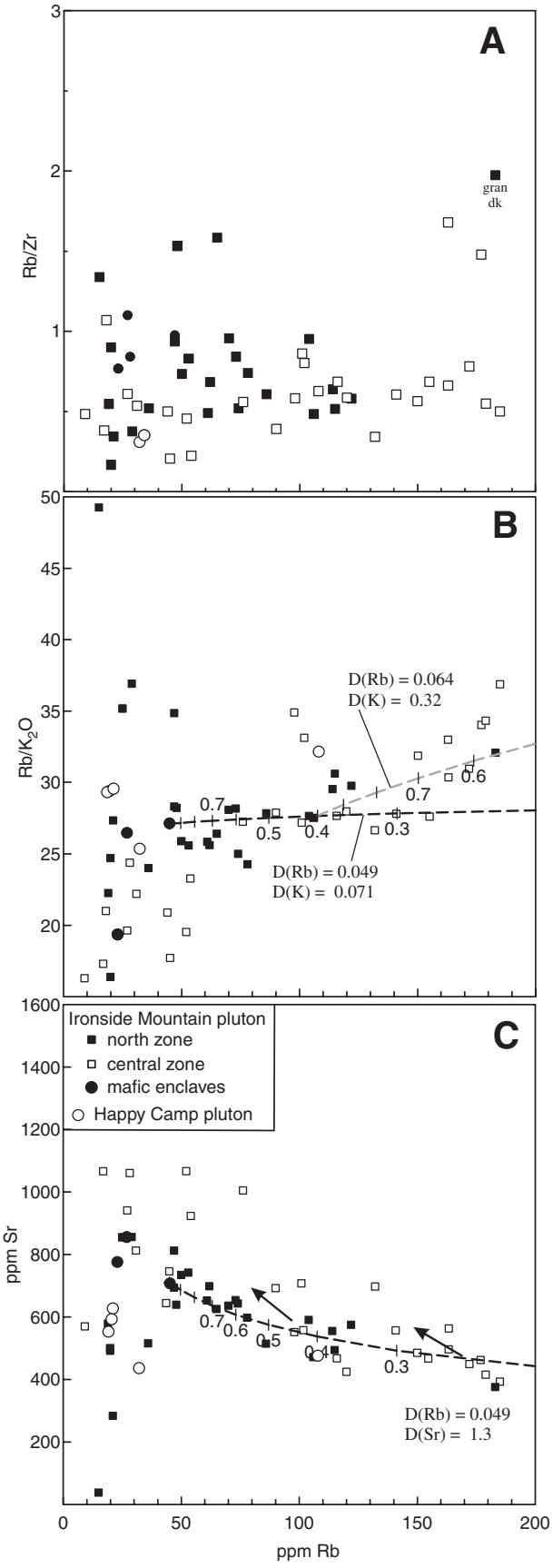

liquid separation ± crystal accumulation. In systems such as the Ironside Mountain pluton, the compositional effects of accumulation can be particularly difficult to determine, because the curvature of compositional trends is not large and there are few fine-grained rocks that might indicate a likely parental composition. The two extreme cases are that the composition of the parental magma was (1) among the most evolved ones observed, so that the compositional trend reflects mixtures of accumulated crystals and trapped liquid (e.g., Charlton, 1979), and (2) among the most mafic ones observed, so that most rock samples represent solidified liquids.

The first case is unlikely, because the mineral assemblage in the most evolved rocks in the pluton is not equivalent to the mineral assemblage in the most mafic rocks, and because plagioclase An contents decrease with increasing bulk rock SiO_2 (see the section on petrography). The second case is also unlikely for the following reasons. First, with few exceptions, major and trace element plots (Figs. 5 and 6) show the most scatter below ~53% SiO_2. At higher SiO_2 contents, most element plots show well-defined trends. This is particularly true for the compatible elements, such as P_2O_5, MnO, V, Zn, and TiO_2, and suggests that the low-SiO_2 rocks consist of variable proportions of accumulated plagioclase and mafic minerals. The plot of Sc versus SiO_2 (Fig. 6F) is especially instructive. The element Sc is strongly compatible in pyroxene and petrographic evidence shows that one or more pyroxenes crystallized at high temperature. Therefore, if the most mafic rocks in the pluton represent parental compositions, they should have the highest Sc contents, and Sc should decrease monotonically with increasing SiO_2. Instead, at low SiO_2 contents, Sc concentrations are approximately constant to ~53% SiO_2 (Fig. 6F). At higher SiO_2 contents, Sc abundances decrease. This pattern suggests that many rocks with <53% SiO_2 are partial cumulates, presumably of a combination of plagioclase and pyroxene, such that the abundance of cumulate plagioclase diluted Sc concentrations. Most of these samples lack quartz and either lack K-feldspar or contain interstitial (rather than poikilitic or subhedral) K-feldspar. In contrast, nearly all samples with ≥53% SiO_2 contain poikilitic

Figure 8. (A) Variation of Rb/Zr ratio as a function of Rb content. (B) Variation of Rb/K_2O as a function of Rb. (C) Variation of Sr as a function of Rb. In B and C, dashed lines represent fractionation models for the Ironside Mountain pluton, assuming a parental basaltic andesite with 45 ppm Rb, 710 ppm Sr, and 1.66 wt% K_2O (equivalent to ~53% SiO_2). This composition is similar to mafic enclave sample OMB1588B (Table 5). Bulk partition coefficients, D, are shown for each element. Tic marks and numbers along the curves represent the fraction of melt remaining. Fractionation of Fe-Ti oxides would not change the shape of the curves but would increase fractionation efficiency (i.e., the space between tic marks would increase). In B and C, the black dashed lines represent a fractionating assemblage of 58% plagioclase, 29% augite, and 13% low-Ca pyroxene. In B, the gray dashed line represents a fractionating assemblage of 55% plagioclase, 5% K-feldspar, 28% augite, and 12% low-Ca pyroxene. In C, arrows indicate the effect of plagioclase accumulation.

to subhedral K-feldspar and interstitial quartz. Thus, the lower SiO_2 samples are interpreted to have lost interstitial melt. In addition to accumulation in the low-SiO_2 samples, a group of samples from the central zone of the pluton also stands out in terms of its higher Na_2O and Sr abundances (Figs. 5 and 6). These higher concentrations are consistent with accumulation of intermediate plagioclase.

Figures 8B and C show simple fractional crystallization models for Rb, Sr, and K_2O in the Ironside Mountain pluton. A fractionating assemblage of plagioclase, augite, and low-Ca pyroxene from a parent with ~53% SiO_2 readily fits the general trend of Rb versus Sr (Fig. 8C). This assemblage also fits the Rb and K_2O data, except among the most differentiated samples (Fig. 8B). These evolved samples can be explained if K-feldspar is added to the fractionating assemblage at Rb contents of ~100 ppm (K_2O contents of ~3.3%). This minor change in assemblage would have no appreciable effect on the trend plotted in Figure 8C.

We conclude that compositional variation in the Ironside Mountain pluton resulted from a combination of fractional crystallization and local accumulation of plagioclase ± pyroxene. The data are consistent with a parental magma similar to mafic enclave OMB1588B (Table 5); a basaltic andesite with ~53% SiO_2, 17.4% Al_2O_3, and 4.3% MgO.

Parental Magma

Discussion of the origin of parental magma(s) for the Ironside Mountain pluton focuses on two themes, the subduction-related origin of the magma and the causes for the parental magma compositions. Figure 7 clearly shows all of the signatures expected of supra-subduction zone magmatism. The rocks are characterized by low abundances of Nb, Ta, and TiO_2 and by high abundances of large ion lithophile elements. The resultant trace element patterns are characteristic of arc magmas and imply a source region modified by transfer of slab-derived fluids and/or melts.

Understanding the origin of the parental magma is more problematic because the rocks do not fit precisely into common pigeonholes for arc magmas. For example, parts or all of the pluton are classified as ferroan or tholeiitic, which is consistent with the inferred low H_2O contents. However, arc tholeiite is generally poor in K_2O and Rb rather than K_2O-rich (e.g., Gill, 1981). In contrast, typical potassic arc magmas (e.g., shoshonites) are defined by magnesian compositions and low FeO/(FeO + MgO) (e.g., Müller and Groves, 1995).

The inferred parental magma has FeO/(FeO + MgO) values too high for the magma to be in equilibrium with a mantle assemblage. This observation is also consistent with its low Cr and Ni contents. In addition, Figures 5 and 6 show that total Fe, TiO_2, Cr, and V all decrease with increasing SiO_2. These trends suggest that, along with plagioclase and pyroxenes, Fe-Ti oxide phases were stable, which indicates that the magma underwent significant differentiation prior to emplacement. This deeper-level differentiation was probably responsible for Fe enrichment and probably involved fractionation of olivine, plagioclase, clinopyroxene, and Cr-spinel from a parental, mantle-derived, low fO_2, low H_2O arc tholeiite. Significant H_2O content would result in evolution along a calc-alkaline line of descent (e.g., Grove and Kinzler, 1986). Finally, low H_2O contents are consistent with the petrographic observation that plagioclase was in reaction with late-stage melts in the Ironside Mountain pluton (e.g., Nekvasil et al., 2000).

This two-stage differentiation scenario is schematically illustrated in Figure 9. If it is correct, then one explanation for the high K_2O content of the magmas arises from experimental studies of Meen (1990). He showed that under relatively low pressure conditions, olivine is the dominant fractionating mafic mineral and that its removal causes SiO_2 enrichment. At higher pressure (8–10 kb), augite fractionation is more important, with consequent increase in abundances of elements such as K_2O and Rb at nearly constant SiO_2 values. The implication of this two-stage differentiation processes is that the mantle-derived magmas must have ponded near the base of relatively thick crust (Fig. 9).

Evidence for a thick Klamath crust during Middle Jurassic time comes from an unusual set of 160-Ma andesitic dikes (Barnes and Allen, this volume). These dikes contain phenocrysts of garnet, plagioclase, Al-rich amphibole, quartz, and epidote. The mineral assemblage and mineral compositions are consistent with equilibration pressures in the 7- to 9-kb range, and the presence of quartz phenocrysts indicates that the assemblage formed in the crust, not in the mantle.

There is no evidence for regional contractional deformation between Ironside Mountain magmatism and emplacement of the garnet-bearing andesite dikes at 160 Ma. Therefore, it is unlikely that crustal thickness increased (except possibly by magmatic underplating) after Ironside Mountain time. Hence, initial high-P (Moho-level?) differentiation of the mantle-derived precursor to the Ironside Mountain parental magma is consistent with available data.

Why Do Wooley Creek Belt Plutons Differ from the Ironside Mountain Pluton?

In the transition from Ironside Mountain magmatism (170–168 Ma) to Wooley Creek belt magmatism (165–156 Ma), magma compositions changed from predominantly K-and Fe-rich, reducing, and H_2O-poor to almost entirely calc-alkaline to calcic, H_2O-rich, and oxidized. Hornblende became an important early phase in crystallization sequences, crustally derived magmas became important parts of the suite, and mixing of mantle and crustal magmas became commonplace (Barnes, 1983; Barnes et al., 1986, 1990, 1995; Gribble et al., 1990). Because Ironside Mountain magmatism followed regional thrusting (Wilson Point thrust) and because no regional contractional deformation separated Ironside Mountain and Wooley Creek belt activity, we surmise that the two magma suites ascended

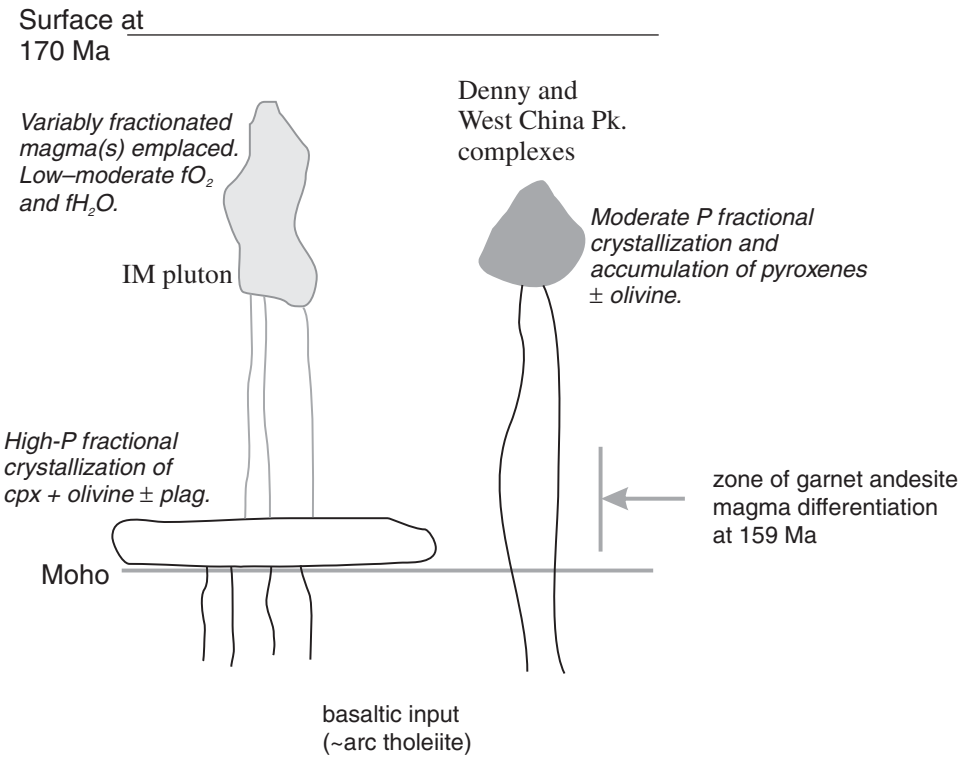

Figure 9. Schematic illustration of the differentiation stages of the Ironside Mountain batholith. Low-fO_2, low-H_2O magmas parental to the Ironside Mountain pluton ponded near the base of the crust. High pressure (7–9 kb) fractionation of augite ± olivine resulted in K_2O enrichment relative to SiO_2. Magmas parental to the Denny and West China Peak complexes were richer in H_2O, had higher fO_2, and underwent little or no differentiation in the deep crust.

through the same structural sequence. Why, then, are they so distinct?

In addition to the possibility of distinct parental magmas (and magma sources), many other explanations have been proposed for the transition from tholeiitic to calc-alkaline magmatism. They include magma mixing (Sakuyama, 1981), increase in H_2O content (Grove and Kinzler, 1986), and crustal contamination (Grove and Baker, 1984; Grove and Kinzler, 1986; but see Hunter, 1998). In the present case, there is evidence that all three explanations are possible: each Wooley Creek belt pluton shows evidence for mixing, predominantly high H_2O contents, and crustal contamination (e.g., Barnes et al., 1990; Gribble et al., 1990; Schmidt, 1994; Johnson and Barnes, this volume). Without discounting the idea of distinct magma source regions, we suggest that these differences also arose because of the changing thermal structure of Klamath Mountain crust from Middle to late Middle Jurassic time.

Because Ironside Mountain magmatism followed regional thrusting, it is likely that the crustal section through which early Ironside Mountain magmas passed was relatively cool and not preconditioned by earlier western Hayfork magmatism. This scenario is supported by the paucity of large western Hayfork-age plutons in the province. As a result, the Ironside Mountain magmas were emplaced into and at the base of a relatively cool crustal section. With succeeding magmatism, the crustal section became hotter and ultimately underwent partial melting during Wooley Creek time.

In this scenario, interaction between the cool crustal section and Ironside Mountain magmas would have been difficult, owing to the amounts of heat necessary to raise crustal temperatures to conditions where assimilation was possible (e.g., Spera and Bohrson, 2001). Instead, these early magmas would have evolved primarily by fractional crystallization ± magma mixing and mingling. However, as the magmatism continued, underplating and intraplating (e.g., Barnes et al., 2002) of mafic magma into the progressively hotter crust would promote melting, hybridization of mantle and crustal magmas, and long-lived magma systems capable of extended open-system behavior.

CONCLUSIONS

Diverse calcic to potassic plutons comprise the Middle Jurassic Ironside Mountain batholith. The Denny and West China Peak complexes range from pyroxenitic to gabbroic and dioritic. Their parental magmas were sufficiently H_2O-rich to support early amphibole stability. The calcic quartz diorite of Happy Camp Mountain was similarly H_2O-rich, but arose from a more evolved parent. The volumetrically important part of the batholith, the 70-km-long Ironside Mountain pluton, is unusual in the Klamath Mountains because it evolved to potassic (quartz monzonitic) compositions. It has petrographic, chemical, and isotopic signatures that suggest approximately closed-system differentiation of an H_2O-poor, low-fO_2 arc tholeiitic parent. Because K_2O enrichment (relative to SiO_2) is difficult at low

pressures, we suggest that such enrichment occurred during early, high pressure fractional crystallization at or just above the base of the crust (≥7 kb).

Emplacement of the Ironside Mountain pluton followed regional thrust faulting. Presumably this contractional deformation reorganized the Klamath crustal sequence so that parental Ironside Mountain magmas entered cool crustal rocks that could not be readily melted or assimilated. With successive magma emplacement during the 165- to 156-Ma Wooley Creek magmatic event, crustal melting ensued and assimilation came to characterize this younger plutonic suite.

ACKNOWLEDGMENTS

We thank Ken Johnson and Greg Harper for helpful discussions and assistance in the field and, particularly, Melanie Barnes for field and laboratory assistance. We also thank Jonathan Miller and Tore Prestvik for their thoughtful reviews and James Hoover for assistance with instrumental neutron activation analyses (University of Texas at El Paso). Our research on the Ironside Mountain pluton, and Klamath magmatism in general, has greatly benefited from the long-term interest and input of Porter Irwin, Bob Coleman, Mary Donato, and Ron Kistler. We thank them all for their help and encouragement. Partial support was provided by National Science Foundation grants EAR-9902912, EAR-9117103, and EAR-8720141.

REFERENCES CITED

Allen, C.M., and Barnes, C.G., 2006, this volume, Ages and some cryptic sources of Mesozoic plutonic rocks in the Klamath Mountains, California and Oregon, *in* Snoke, A.W., and Barnes, C.G., eds., Geological studies in the Klamath Mountains province, California and Oregon: A volume in honor of William P. Irwin: Boulder, Colorado, Geological Society of America Special Paper 410, doi: 10.1130/2006.2410(11).

Anderson, A.T., 1976, Magma mixing: Petrological process and volcanological tool: Journal of Volcanology and Geothermal Research, v. 1, p. 3–33, doi: 10.1016/0377-0273(76)90016-0.

Anderson, J.L., and Smith, D.R., 1995, The effects of temperature and fO_2 on the Al-in-hornblende barometer: American Mineralogist, v. 80, p. 549–559.

Barnes, C.G., 1983, Petrology and upward zonation of the Wooley Creek batholith, Klamath Mountains, California: Journal of Petrology, v. 24, p. 495–537.

Barnes, C.G., and Allen, C.M., 2006, this volume, Depth of origin of late Middle Jurassic garnet andesite, southern Klamath Mountains, California, *in* Snoke, A.W., and Barnes, C.G., eds., Geological studies in the Klamath Mountains province, California and Oregon: A volume in honor of William P. Irwin: Boulder, Colorado, Geological Society of America Special Paper 410, doi: 10.1130/2006.2410(13).

Barnes, C.G., Allen, C.M., and Saleeby, J.B., 1986, Open- and closed-system characteristics of a tilted plutonic system, Klamath Mountains, California: Journal of Geophysical Research, v. 91, p. 6073–6090.

Barnes, C.G., Allen, C.M., Hoover, J.D., and Brigham, R.H., 1990, Magmatic components of a tilted plutonic system, Klamath Mountains, California, *in* Anderson, J.L., ed., The nature and origin of Cordilleran magmatism: Boulder, Colorado, Geological Society of America Memoir 174, p. 331–346.

Barnes, C.G., Petersen, S.W., Kistler, R.W., Prestvik, T., and Sundvoll, B., 1992, Tectonic implications of isotopic variation among Jurassic and early Cretaceous plutons, Klamath Mountains: Geological Society of America Bulletin, v. 104, p. 117–126, doi: 10.1130/0016-7606(1992)104<0117:TIOIVA>2.3.CO;2.

Barnes, C.G., Johnson, K., Barnes, M.A., Prestvik, T., Kistler, R.W., and Sundvoll, B., 1995, The Grayback pluton: Magmatism in a Jurassic back-arc environment, Klamath Mountains, Oregon: Journal of Petrology, v. 36, p. 397–415.

Barnes, C.G., Petersen, S.W., Kistler, R.W., Murray, R., and Kays, M.A., 1996, Source and tectonic implications of tonalite-trondhjemite magmatism in the Klamath Mountains: Contributions to Mineralogy and Petrology, v. 123, p. 40–60, doi: 10.1007/s004100050142.

Barnes, C.G., Yoshinobu, A., Prestvik, T., Nordgulen, Ø., Karlsson, H., and Sundvoll, B., 2002, Mafic magma intraplating: Anatexis and hybridization in arc crust, Bindal Batholith, Norway: Journal of Petrology, v. 43, p. 2171–2190, doi: 10.1093/petrology/43.12.2171.

Barnes, C.G., Snoke, A.W., Harper, G.D., Frost, C.D., McFadden, R.R., Bushey, J.C., and Barnes, M.A.W., 2006, this volume (Chapter 17), Arc plutonism following regional thrusting: Petrology and geochemistry of syn- and post-Nevadan plutons in the Siskiyou Mountains, Klamath Mountains province, California, *in* Snoke, A.W., and Barnes, C.G., eds., Geological studies in the Klamath Mountains province, California and Oregon: A volume in honor of William P. Irwin: Boulder, Colorado, Geological Society of America Special Paper 410, doi: 10.1130/2006.2410(17).

Beard, J.S., 1986, Characteristic mineralogy of arc-related cumulate gabbros: Implications for the tectonic setting of gabbroic plutons and for andesite genesis: Geology, v. 14, p. 848–851, doi: 10.1130/0091-7613(1986)14<848:CMOACG>2.0.CO;2.

Bushey, J.C., Snoke, A.W., Barnes, C.G., and Frost, C.D., 2006, this volume, Geology of the Bear Mountain intrusive complex, Klamath Mountains, California, *in* Snoke, A.W., and Barnes, C.G., eds., Geological studies in the Klamath Mountains province, California and Oregon: A volume in honor of William P. Irwin: Boulder, Colorado, Geological Society of America Special Paper 410, doi: 10.1130/2006.2410(14).

Charlton, D.W., 1979, Geology of part of the Ironside Mountian quadrangle, northern California, Klamath Mountains [Ph.D. dissertation]: Santa Barbara, University of California, 542 pp.

Cotkin, S.J., and Medaris, L.G., Jr., 1993, Evaluation of the crystallization conditions for the calcalkaline Russian Peak intrusive complex, Klamath Mountains, northern California: Journal of Petrology, v. 34, p. 543–571.

Donato, M.M., Barnes, C.G., and Gray, G.G., 1983, Geologic map of the Orleans Mountain roadless area, Humboldt and Siskiyou Counties, California: Reston, Virginia, U.S. Geological Survey Miscellaneous Field Investigations Map MF-1526-A, scale, 1:62,500, 1 oversized sheet.

Donato, M.M., Barnes, C.G., and Tomlinson, S.L., 1996, The enigmatic Applegate Group of southwestern Oregon: Age, correlation, and tectonic affinity: Oregon Geology, v. 58, p. 79–91.

Ernst, W.G., 1998, Geology of the Sawyers Bar area, Klamath Mountains, northern California: Sacramento, California Division of Mines and Geology Map Sheet 47, scale 1:48,000, 1 sheet, 59 p.

Frost, B.R., Barnes, C.G., Collins, W.J., Arculus, R.J., Ellis, D.J., and Frost, C.D., 2001, A geochemical classification for granitic rocks: Journal of Petrology, v. 42, p. 2033–2048.

Gill, J., 1981, Orogenic andesites and plate tectonics: New York, Springer-Verlag, 390 pp.

Goldstein, S.L., O'Nions, R.K., and Hamilton, P.J., 1984, A Sm-Nd isotopic study of atmospheric dusts and particulates from major river systems: Earth and Planetary Science Letters, v. 70, p. 221–236, doi: 10.1016/0012-821X(84)90007-4.

Gray, G.G., 1986, Native terranes of the central Klamath Mountains, California: Tectonics, v. 5, p. 1043–1054.

Gribble, R.F., Barnes, C.G., Donato, M.M., Hoover, J.D., and Kistler, R.W., 1990, Geochemistry and intrusive history of the Ashland pluton, Klamath Mountains, California and Oregon: Journal of Petrology, v. 31, p. 883–923.

Grove, T.L., and Baker, M.B., 1984, Phase equilibrium controls on the tholeiitic versus calc-alkaline differentiation trends: Journal of Geophysical Research, v. 89, p. 3252–3274.

Grove, T.L., and Kinzler, R.J., 1986, Petrogenesis of andesites: Annual Review of Earth and Planetary Sciences, v. 14, p. 417–454, doi: 10.1146/annurev.ea.14.050186.002221.

Hacker, B.R., Donato, M.M., Barnes, C.G., McWilliams, M.O., and Ernst, W.G., 1995, Timescales of orogeny: Jurassic construction of the Klamath Mountains: Tectonics, v. 14, p. 677–703, doi: 10.1029/94TC02454.

Hammarstrom, J.M., and Zen, E., 1986, Aluminum in hornblende: An empirical igneous geobarometer: American Mineralogist, v. 71, p. 1297–1313.

Harper, G.D., and Wright, J.E., 1984, Middle to Late Jurassic tectonic evolution of the Klamath Mountains, California-Oregon: Tectonics, v. 3, p. 759–772.

Harper, G.D., Saleeby, J.B., and Heizler, M., 1994, Formation and emplacement of the Josephine ophiolite and the Nevadan orogen in the Klamath Mountains, California-Oregon: U/Pb zircon and $^{40}Ar/^{39}Ar$ geochronology: Journal of Geophysical Research, v. 99, p. 4293–4321, doi: 10.1029/93JB02061.

Hollister, L.S., Grissom, G.C., Peters, E.K., Stowell, H.H., and Sisson, V.B., 1987, Confirmation of the empirical correlation of Al in hornblende with pressure of solidification of calc-alkaline plutons: American Mineralogist, v. 72, p. 231–239.

Hotz, P.E., 1971, Plutonic rocks of the Klamath Mountains, California and Oregon: Washington, D.C., U.S. Geological Survey Professional Paper 684-B, p. 1–20.

Hunter, A.G., 1998, Intracrustal controls on the coexistence of tholeiitic and calc-alkaline magma series at Aso Volcano, SW Japan: Journal of Petrology, v. 39, p. 1255–1284, doi: 10.1093/petrology/39.7.1255.

Irwin, W.P., 1960, Geologic reconnaissance of the northern Coast Ranges and Klamath Mountains, California, with a summary of the mineral resources: San Francisco, Bulletin of the California Division of Mines and Geology 179, 80 pp.

Irwin, W.P., 1972, Terranes of the western Paleozoic and Triassic belt in the southern Klamath Mountains, California: Washington, D.C., U.S. Geological Survey Professional Paper 800-C, p. 103–111.

Irwin, W., and Wooden, J., 1999, Plutons and accretionary episodes of the Klamath Mountains, California and Oregon: Reston, Virginia, U.S. Geological Survey Open-File Report 99-374, 1 sheet.

Johnson K., and Barnes, C.G., 2006, this volume, Magma mixing and mingling in the Grayback pluton, Klamath Mountains, Oregon, *in* Snoke, A.W., and Barnes, C.G., eds., Geological studies in the Klamath Mountains province, California and Oregon: A volume in honor of William P. Irwin: Boulder, Colorado, Geological Society of America Special Paper 410, doi: 10.1130/2006.2410(12).

Kistler, R.W., Chappell, B.W., Peck, D.L., and Bateman, P.C., 1986, Isotopic variation in the Tuolumne Intrusive Suite, central Sierra Nevada, California: Contributions to Mineralogy and Petrology, v. 94, p. 205–220, doi: 10.1007/BF00592937.

Kuno, H., 1968, Differentiation of basalt magmas, *in* Hess, H.H., and Poldevaart, A., eds., Basalts, vol. II: New York, Wiley Intersciences Publications, p. 624–688.

Lanphere, M.A., Irwin, W.P., and Hotz, P.E., 1968, Isotopic age of the Nevadan orogeny and older plutonic and metamorphic events in the Klamath Mountains, California: Geological Society of America Bulletin, v. 79, p. 1027–1052.

Leake, B., Woolley, A., Arps, C., Birch, W., Gilbert, M., Grice, J., Hawthorne, F., Kato, A., Kisch, H., Krivovichev, V., Linthout, K., Laird, J., Mandarino, J., Schumacher, J., Smith, D., Stephenson, N., Ungaretti, L., Whittaker, E., and Youzhi, G., 1997, Nomenclature of amphiboles: Report of the Subcommittee on Amphiboles of the International Mineralogical Association, Commission on New Minerals and Mineral Names: American Mineralogist, v. 82, p. 1019–1037.

Le Maitre, R.W., Streckeisen, A., Zanettin, B., Le Bas, M.J., Bonin, B., Bateman, P., Bellieni, G., Dudek, A., Efremova, S., Keller, J., Lameyre, J., Sabine, P.A., Schmid, R., Sorensen, H., and Woolley, A.R., 2002, Igneous Rocks: A classification and glossary of terms, recommendations of the International Union of Geological Sciences Subcommission on the Systematics of Igneous Rocks (2nd edition): Cambridge, Cambridge University Press, 252p.

MacDonald, G.A., and Katsura, T., 1964, Chemical composition of Hawaiian lavas: Journal of Petrology, v. 5, p. 83–133.

Mars, E.V., 1999, Petrology and geochemistry of the Ironside Mountain batholith, Klamath Mountains, northern California [MS thesis]: Lubbock, Texas Tech University, 71 pp.

Masi, U., O'Neil, J.R., and Kistler, R.W., 1981, Stable isotope systematics in Mesozoic granites of central and northern California and southwestern Oregon: Contributions to Mineralogy and Petrology, v. 76, p. 116–126, doi: 10.1007/BF00373691.

Meen, J.K., 1990, Elevation of potassium content of basaltic magma by fractional crystallization: The effect of pressure: Contributions to Mineralogy and Petrology, v. 104, p. 309–331, doi: 10.1007/BF00321487.

Middlemost, E.A.K., 1975, The basalt clan: Earth Science Reviews, v. 11, p. 337–364, doi: 10.1016/0012-8252(75)90039-2.

Miller, J., Miller, R., Wooden, J., and Harper, G., 2003, Geochronologic links between the Ingalls ophiolite, North Cascades, Washington and the Josephine ophiolite, Klamath Mts., Oregon and California: Geological Society of America Abstracts with Programs, v. 35, p. 113.

Miyashiro, A., 1974, Volcanic rock series in island arcs and active continental margins: American Journal of Science, v. 274, p. 321–355.

Moore, J.G., 1959, The quartz diorite boundary line in the western United States: Journal of Geology, v. 67, p. 198–210.

Müller, D., and Groves, D.I., 1995, Potassic igneous rocks and associated gold-copper mineralization: New York, Springer-Verlag, 252 pp.

Nekvasil, H., and Lindsley, D.H., 1990, Termination of the 2 feldspar + liquid curve in the system Ab-Or-An-H_2O at low H_2O contents: American Mineralogist, v. 75, p. 1071–1079.

Nekvasil, H., Simon, A., and Lindsley, D.H., 2000, Crystal fractionation and the evolution of intra-plate *hy*-normative igneous suites: Insights from the feldspars: Journal of Petrology, v. 41, p. 1743–1757, doi: 10.1093/petrology/41.12.1743.

Rickwood, P.C., 1989, Boundary lines within petrologic diagrams which use oxides of major and minor elements: Lithos, v. 22, p. 247–263, doi: 10.1016/0024-4937(89)90028-5.

Sakuyama, M., 1981, Petrological study of the Myoko and Kurohime volcanoes, Japan: Crystallization sequence and evidence for magma mixing: Journal of Petrology, v. 22, p. 553–583.

Saleeby, J.B., Harper, G.D., Snoke, A.W., and Sharp, W.D., 1982, Time relations and structural-stratigraphic patterns in ophiolite accretion, west-central Klamath Mountains, California: Journal of Geophysical Research, v. 87, no. B5, p. 3831–3848.

Schmidt, B.L., 1994, The petrology and geochemistry of the English Peak intrusive suite, Klamath Mountains, California [Ph.D. dissertation]: Lubbock, Texas Tech University, 216 p.

Schmidt, M.W., 1992, Amphibole composition in tonalite as a function of pressure: An experimental calibration of the Al-in-hornblende barometer: Contributions to Mineralogy and Petrology, v. 110, p. 304–310, doi: 10.1007/BF00310745.

Shannon, W.M., Barnes, C.G., and Bickford, M.E., 1997, Grenville magmatism in west Texas: Petrology and geochemistry of the Red Bluff granitic suite: Journal of Petrology, v. 38, p. 1279–1305, doi: 10.1093/petrology/38.10.1279.

Sisson, T.W., and Grove, T.L., 1993, Experimental investigations of the role of H_2O in calc-alkaline differentiation and subduction zone magmatism: Contributions to Mineralogy and Petrology, v. 113, p. 143–166, doi: 10.1007/BF00283225.

Snoke, A.W., Quick, J.E., and Bowman, H.R., 1981, Bear Mountain igneous complex, Klamath Mountains, California: An ultrabasic to silicic calc-alkaline suite: Journal of Petrology, v. 22, p. 501–552.

Spera, F., and Bohrson, W., 2001, Energy-constrained open-system magmatic

processes I: General model and energy-constrained assimilation and fractional crystallization (EC-AFC) formulation: Journal of Petrology, v. 42, p. 999–1018, doi: 10.1093/petrology/42.5.999.

Sun, S.-s., and McDonough, W.F., 1989, Chemical and isotopic systematics of oceanic basalts: Implications for mantle composition and processes, *in* Saunders, A., and Norry, M., eds., Magmatism in the ocean basins: Oxford, Geological Society Special Publication, p. 313–345.

Treuil, M., Joron, J.L., and Jaffrezic, H., 1977, Trace element geochemistry of magmatic rock series of converging and diverging plate boundaries: Journal of Radioanalytical Chemistry, v. 38, p. 351–362.

Wright, J.E., 1982, Permo-Triassic accretionary subduction complex, southwestern Klamath Mountians, northern California: Journal of Geophysical Research, v. 87, p. 3805–3818.

Wright, J.E., and Fahan, M.R., 1988, An expanded view of Jurassic orogenesis in the western United States Cordillera: Middle Jurassic (pre-Nevadan) regional metamorphism and thrust faulting within an active arc environment, Klamath Mountains, California: Geological Society of America Bulletin, v. 100, p. 859–876, doi: 10.1130/0016-7606(1988)100<0859:AEVOJO>2.3.CO;2.

Wright, J.E., and Wyld, S.J., 1994, The Rattlesnake Creek terrane, Klamath Mountains, California: An early Mesozoic volcanic arc and its basement of tectonically disrupted oceanic crust: Geological Society of America Bulletin, v. 106, p. 1033–1056, doi: 10.1130/0016-7606(1994)106<1033:TRCTKM>2.3.CO;2.

Young, J.C., 1978, Geology of the Willow Creek quadrangle, Humboldt and Trinity Counties, California: San Francisco, California Division of Mines and Geology, Map Sheet 31, scale 1:62,500, 1 sheet, 16 p.

Yule, J.D., Saleeby, J.B., and Barnes, C.G., 2006, this volume, A rift-edge facies of the Late Jurassic Rogue–Chetco arc and Josephine ophiolite, Klamath Mountains, Oregon, *in* Snoke, A.W., and Barnes, C.G., eds., Geological studies in the Klamath Mountains province, California and Oregon: A volume in honor of William P. Irwin: Boulder, Colorado, Geological Society of America Special Paper 410, doi: 10.1130/2006.2410(03).

Manuscript Accepted by the Society 10 January 2006

Printed in the USA

Geological Society of America Special Papers

Petrology and geochemistry of the Middle Jurassic Ironside Mountain batholith: Evolution of potassic magmas in a primitive arc setting

Calvin G. Barnes, Elizabeth V. Mars, Susan Swapp, et al.

Geological Society of America Special Papers 2006;410; 199-221
doi:10.1130/2006.2410(10)